

# A HST/COS survey of molecular hydrogen in DLAs & sub-DLAs at $z < 1$ : Molecular fraction and excitation temperature<sup>\*</sup>

S. Muzahid<sup>1</sup>†, R. Srianand<sup>2</sup>, and J. Charlton<sup>1</sup>

<sup>1</sup> *The Pennsylvania State University, 525 Davey Lab, University Park, State College, PA 16802, USA*

<sup>2</sup> *Inter-University Centre for Astronomy and Astrophysics, Post Bag 4, Ganeshkhind, Pune 411007, India*

Accepted. Received; in original form

## ABSTRACT

We present the results of a systematic search for molecular hydrogen ( $\text{H}_2$ ) in low redshift ( $0.05 \lesssim z \lesssim 0.7$ ) damped and sub-damped  $\text{Ly}\alpha$  absorption systems (DLAs/sub-DLAs) with  $N(\text{H I}) \gtrsim 10^{19.0} \text{ cm}^{-2}$ , in the archival *Hubble Space Telescope* (*HST*)/Cosmic Origins Spectrograph (COS) spectra. Our core sample is comprised of 27 systems with a median  $\log N(\text{H I}) = 19.6$ . This is a factor of  $\sim 10$  lower than that of the high- $z$  ( $z > 2$ ) sample of Noterdaeme et al.  $\text{H}_2$  absorption is detected in 10 cases (3/5 in DLAs and 7/22 in sub-DLAs). On the average, our survey is sensitive down to  $\log N(\text{H}_2) = 14.4$  corresponding to a molecular mass fraction of  $\log f_{\text{H}_2} = -4.9$  at the median  $N(\text{H I})$ . The  $\text{H}_2$  incidence rate of  $50_{-12}^{+25}$  percent, is a factor of  $\gtrsim 2$  higher than that of the high- $z$  sample, for systems with  $N(\text{H}_2) > 10^{14.4} \text{ cm}^{-2}$ . The enhanced incidence rate could result from the increase of the cosmic mean metallicities of DLAs and sub-DLAs with cosmic time. In spite of having systematically lower  $N(\text{H I})$  values, low- $z$   $\text{H}_2$  systems show molecular mass fractions ( $\log f_{\text{H}_2} = -1.93 \pm 0.63$ ) that are comparable to the high- $z$  measurements. The rotational excitation temperatures ( $T_{01} = 133 \pm 55 \text{ K}$ ), as measured in our low- $z$  sample, are typically consistent with high- $z$  measurements. Simple photoionization models demonstrate that the radiation field prevailing in the low- $z$   $\text{H}_2$  systems cannot have an appreciable stellar contribution for densities of  $10 - 100 \text{ cm}^{-3}$ . The impact parameters of the nearest possible host-galaxy candidates are typically large (e.g.  $10 \lesssim \rho \text{ (kpc)} \lesssim 80$ ). We, therefore, conjecture that the low- $z$   $\text{H}_2$  bearing gas is not related to star-forming disks but stems from self-shielded, tidally stripped or ejected disk-material in the extended halo.

**Key words:** galaxies: ISM – galaxies: haloes – quasar: absorption line

## 1 INTRODUCTION

Damped  $\text{Ly}\alpha$  absorbers (DLAs) and sub-DLAs seen in QSO spectra are characterized by very high neutral hydrogen column densities:  $N(\text{H I}) \geq 1 \times 10^{19} \text{ cm}^{-2}$  for sub-DLAs and  $> 2 \times 10^{20} \text{ cm}^{-2}$  for DLAs (see Wolfe et al. 2005, for a review). Whereas the ionization correction can be appreciable in sub-DLAs (Péroux et al. 2003a,b), DLAs are predominantly neutral and form the major reservoirs of neutral-gas at high redshift (Prochaska & Wolfe 2009; Noterdaeme et al. 2009b, 2012b). In general, DLAs/sub-DLAs show higher metallicities compared to the  $\text{Ly}\alpha$  forest systems (Schaye et al. 2003; Wolfe et al. 2005; Kulkarni et al. 2005). An increase in the cosmic mean metallicity

of DLAs/sub-DLAs with cosmic time has been reported (see e.g. Prochaska et al. 2003; Kulkarni et al. 2007; Rafelski et al. 2012; Som et al. 2013). Moreover, DLA metallicities are found to be correlated with the velocity spread ( $\Delta v_{90}$ ) of neutral or singly ionized metal lines (Ledoux et al. 2006a), which has been interpreted as the mass-metallicity relation seen in galaxies (Tremonti et al. 2004). All these suggest that the DLAs/sub-DLAs are located in overdense regions where star formation activity takes place (see e.g. Pettini et al. 1997). Direct detections of  $\text{Ly}\alpha/\text{H}\alpha/[\text{O III}]$  emission lines in a handful of DLAs (Møller et al. 2004; Fynbo et al. 2010; Péroux et al. 2011; Noterdaeme et al. 2012a; Jorgenson & Wolfe 2014) made such an idea more compelling. Absorption studies of DLA/sub-DLA systems, thus, provide a unique means to probe galaxy neighbourhoods over a wide range of redshift ( $0 < z < 5$ ) without the biases introduced in magnitude limited sample of galaxies studied in emission.

The connection between DLAs/sub-DLAs and galaxies can be firmly established either by directly detecting galaxies at the

<sup>\*</sup> Based on observations made with the NASA/ESA Hubble Space Telescope, obtained from the data archive at the Space Telescope Science Institute, which is operated by the Association of Universities for Research in Astronomy, Inc., under NASA contract NAS 5-26555.  
<sup>†</sup> E-mail: sowgatm@gmail.com

same redshifts and/or by showing that the physical conditions in the absorbing gas are consistent with those seen in a typical galactic interstellar medium (ISM). Except the previously mentioned few cases, direct detections of candidate galaxies hosting DLAs or sub-DLAs at  $z > 1.7$  have not been very successful (Kulkarni et al. 2006; Christensen et al. 2007). Thus, our understanding of the physical conditions in high- $z$  DLAs/sub-DLAs primarily relies on the optical absorption-line spectroscopy using low-ionization metal lines and, in a few cases, H<sub>2</sub>, HD, and CO molecular absorption (e.g. Ledoux et al. 2003; Srianand et al. 2005, 2008; Noterdaeme et al. 2008a,b, 2009a, 2010; Tumlinson et al. 2010; Guimarães et al. 2012; Albornoz Vásquez et al. 2014). At low redshift ( $z < 1$ ) it is relatively easy to detect candidate host-galaxies in most cases.

Molecular hydrogen (H<sub>2</sub>) is the most abundant molecule in the universe which also acts as the most important molecular coolant. Formation of H<sub>2</sub> is expected on the surface of dust grains if the gas is cool, dense and mostly neutral (Gould & Salpeter 1963; Hollenbach & Salpeter 1971). In the case of warm and dust-free gas, H<sub>2</sub> can form via H<sup>-</sup> ions (Jenkins & Peimbert 1997). Photodissociation of H<sub>2</sub> takes place in the energy range 11.1–13.6 eV via Lyman- and Warner-band absorption lines. Therefore, information on the kinetic and rotational excitation temperatures, the particle density, and the radiation field can be derived from good quality data when H<sub>2</sub> is detected. For example, at high redshift, DLA subcomponents in which H<sub>2</sub> absorption is detected have typical kinetic temperature of  $T = 153 \pm 78$  K and density of  $n_{\text{H}} = 10\text{--}200$  cm<sup>-3</sup> (Srianand et al. 2005). The typical inferred radiation field in the H<sub>2</sub> bearing components is of the order of the mean UV radiation field in the Galactic ISM. Systematic surveys at high redshift ( $z > 1.7$ ) have shown that the H<sub>2</sub> is detected in 10–20% of DLAs/sub-DLAs (see e.g. Ledoux et al. 2003; Noterdaeme et al. 2008a). H<sub>2</sub> content is typically low and is found to be proportional to the metallicity and dust depletion, in those studies. The frequent detections of molecular hydrogen towards dusty and high-metallicity regions hints at its connection to star-forming regions (see also Petitjean et al. 2006).

In spite of having enormous diagnostic potential to probe physical conditions in galaxies in a luminosity unbiased way, molecular hydrogen has not been well studied at low- $z$ . This is primarily because the atmospheric cutoff of light below 3000 Å makes ground-based observations of H<sub>2</sub> impossible for redshift  $z < 1.7$ . In addition, due to the unavailability of high resolution UV sensitive spectrographs in the past, our knowledge of molecular content of galaxies (probed by DLAs/sub-DLAs) beyond the Magellanic clouds and below  $z < 1.7$  remains very poor. This is the same redshift range over which the evolution of cosmic density of neutral gas,  $\Omega_{\text{HI}}$ , is highly debated (Rao & Turnshek 2000). As  $\Omega_{\text{HI}}$  evolution is thought to be controlled by star-formation activity that is tightly coupled to the physical state of the H I gas, it is of utmost importance to study H<sub>2</sub> in this redshift range. The high throughput of HST/COS FUV gratings gives us a window of opportunity to explore this redshift range now. The numerous UV absorption lines of H<sub>2</sub> from different rotational ( $J$ ) levels are now accessible for absorbers with redshift as low as  $z \sim 0.05$  in HST/COS spectra (see e.g. Crighton et al. 2013; Oliveira et al. 2014; Srianand et al. 2014). Here we present the results of our systematic search for low- $z$  molecular hydrogen in DLAs/sub-DLAs that are detected in the medium resolution COS spectra from the HST archive.

This article is organized as follows. In Section 2 we discuss the observations and reduction of the spectra we have used to search for H<sub>2</sub> systems. In Section 3 we describe our search technique, final

data sample, and the absorption line measurements. Detailed analysis of the sample is presented in Section 4. In Section 5 we discuss our results. The important findings are summarized in Section 6. Throughout this work we assume a flat  $\Lambda$ CDM cosmology with  $H_0 = 70$  km s<sup>-1</sup> Mpc<sup>-1</sup>,  $\Omega_{\text{M}} = 0.3$ , and  $\Omega_{\Lambda} = 0.7$ . The wavelengths of H<sub>2</sub> transitions are taken from Bailly et al. (2010).

## 2 OBSERVATIONS AND DATA REDUCTION

We have searched for DLAs and sub-DLAs in nearly 400 far-ultraviolet (FUV) spectra of intermediate redshift quasars, observed with the HST/COS, that were available in the public HST archive before March, 2014. The properties of COS and its in-flight operations are discussed by Osterman et al. (2011) and Green et al. (2012). All the COS spectra were obtained using medium resolution ( $R \sim 20,000$ ) FUV COS gratings (G130M and/or G160M). The data were retrieved from the HST archive and reduced using the CALCOS pipeline software. The pipeline reduced data (so called “*x1d*” files) were flux calibrated. To increase the spectral signal-to-noise ratio (SNR), individual G130M and G160M integrations were aligned and coadded using the IDL code (“*coadd\_x1d*”) developed by Danforth et al. (2010)<sup>1</sup>. The exposures were weighted by the integration time while coadding in flux units. Since our data comes from different observing programs, the final data sample show a range in spectral SNR (e.g.  $\sim 5$  to 25 per resolution element). As the COS FUV spectra are significantly oversampled (i.e. six raw pixels per resolution element), we binned the data by three pixels. This further improves SNR per pixel. All our measurements and analyses were, subsequently, performed on the binned data. Measurements are, however, found to be fairly independent of binning. Continuum normalization was done by fitting the line-free regions with a smooth lower-order polynomial.

## 3 SEARCH TECHNIQUE, DATA SAMPLE, AND ABSORPTION LINE MEASUREMENTS

We have conducted a systematic search for DLAs and sub-DLAs in nearly 400 HST/COS spectra. Identifying DLAs/sub-DLAs is fairly straightforward in intermediate redshift QSO spectra as they produce distinct damping wings in the Ly $\alpha$  absorption and as there is no Ly $\alpha$  forest crowding at low- $z$  (see e.g. Fig. 1). Note that, Ly $\alpha$  absorption will only be covered by the COS spectra for systems with  $0 < z_{\text{abs}} < 0.47$ , provided both G130M and G160M data are available. With the G130M data alone, Ly $\alpha$  can be covered up to  $0 < z_{\text{abs}} \lesssim 0.19$ . Therefore, in order to account for the systems for which Ly $\alpha$  absorption is not covered, we searched for systems that produce a strong Lyman limit ( $\lambda_{\text{rest}} = 912$  Å) break or show strong Lyman series lines as shown in the right panel of Fig. 1. In total we have found 33 systems with  $\log N(\text{H I}) \gtrsim 19.0$  as listed by increasing absorption redshift ( $z_{\text{abs}}$ ) in Table 1 & 2. Our core sample, for which Lyman and Werner band absorption lines of H<sub>2</sub> are covered by the COS spectra, is comprised of the 27 systems that are listed in Table 1. In Table 2 we have listed six other systems with  $\log N(\text{H I}) \gtrsim 19.0$  for which H<sub>2</sub> information is not available in the existing spectra.

For every identified DLAs/sub-DLAs in Table 1, we have searched for the Lyman and Werner band absorption lines from

<sup>1</sup> <http://casa.colorado.edu/danforth/science/cos/costools.html>

**Table 1.** Core sample of low- $z$  DLAs/sub-DLAs for which  $H_2$  information is available.

QSO	$z_{\text{em}}$	PID	PI	$z_{\text{abs}}$	$\log N(\text{H I})$	$H_2$ Status	$N(\text{H}_2)^1$ Sensitivity	$\log N(\text{H}_2)^2$	$\log f_{\text{H}_2}^3$	$\rho^4$ (kpc)
(1)	(2)	(3)	(4)	(5)	(6)	(7)	(8)	(9)	(10)	(11)
PG1216+069	0.331	12025	J. Green	0.00635	$19.32 \pm 0.03^a$	NO	17.8	$< 17.8^a$	$< -1.24^a$	$121^a$
MRK486	0.039	12276	B. Wakker	0.03879	$20.25 \pm 0.25$	NO	15.6	$< 15.6$	$< -4.35$	
J1241+2852	0.589	12603	T. Heckman	0.06650	$19.18 \pm 0.10$	YES	14.9	$16.45 \pm 0.12$	$-2.43 \pm 0.16$	
J1553+3548	0.723	11598	J. Tumlinson	0.08300	$19.55 \pm 0.15^b$	NO	14.6	$< 14.6$	$< -4.65$	
J1619+3342	0.472	11598	J. Tumlinson	0.09630	$20.55 \pm 0.10^b$	YES	14.4	$18.57 \pm 0.06^c$	$-1.69 \pm 0.11^c$	$14^c$
Q0439-433	0.594	12536	V. Kulkarni	0.10115	$19.63 \pm 0.08$	YES	14.2	$16.64 \pm 0.05$	$-2.69 \pm 0.09$	8 (Pet96)
J0928+6025	0.296	11598	J. Tumlinson	0.15380	$19.35 \pm 0.15^b$	NO	14.5	$< 14.5$	$< -4.55$	91 (Wer13)
PHL1226	0.404	12536	V. Kulkarni	0.15962	$19.37 \pm 0.10$	NO	14.3	$< 14.3$	$< -4.77$	
Q0850+440	0.515	13398	C. Churchill	0.16375	$19.67 \pm 0.10^d$	YES	13.9	$15.05 \pm 0.07$	$-4.32 \pm 0.12$	24 (Kac11)
B0120-28	0.434	12204	C. Thom	0.18562	$20.50 \pm 0.10^e$	YES	13.9	$20.00 \pm 0.10^e$	$-0.41 \pm 0.12^e$	$70^e$
J1435+3604	0.430	11598	J. Tumlinson	0.20260	$19.80 \pm 0.10^b$	NO	14.4	$< 14.4$	$< -5.10$	39 (Wer13)
J1342-0053	0.326	11598	J. Tumlinson	0.22711	$19.0^{+0.5}_{-0.8}^f$	YES	14.2	$14.63 \pm 0.06$	$-4.07^{+0.50}_{-0.80}$	35 (Wer13)
J0925+4004	0.472	11598	J. Tumlinson	0.24788	$19.55 \pm 0.15^b$	YES	14.6	$18.82 \pm 0.13$	$-0.57 \pm 0.17$	83 (Wer13)
J1001+5944	0.747	12248	J. Tumlinson	0.30350	$19.32 \pm 0.10^g$	NO	14.1	$< 14.1$	$< -4.92$	
J1616+4154	0.441	11598	J. Tumlinson	0.32110	$20.60 \pm 0.20^b$	YES	14.2	$19.26 \pm 0.09$	$-1.08 \pm 0.20$	Not found <sup>g</sup>
Q1323+343	0.443	12593	D. Nestor	0.35300	$18.92 \pm 0.20$	NO	14.5	$< 14.5$	$< -4.12$	
Q1400+553	0.840	12593	D. Nestor	0.36475	$20.11 \pm 0.20$	NO	14.5	$< 14.5$	$< -5.31$	
J0209-0438	1.132	12264	S. Morris	0.39055	$19.00 \pm 0.12^h$	NO	14.0	$< 14.0$	$< -4.70$	
Q1232-022	1.043	12593	D. Nestor	0.39495	$20.79 \pm 0.20$	NO	14.8	$< 14.8$	$< -5.69$	
Q1251+463	1.460	12593	D. Nestor	0.39662	$20.50 \pm 0.20$	NO	14.4	$< 14.4$	$< -5.80$	
Q0454-2203	0.533	12466	J. Charlton	0.47437	$19.97 \pm 0.15^i$	NO	14.0	$< 14.0$	$< -5.67$	
Q0454-2203	0.533	12466	J. Charlton	0.48321	$19.59 \pm 0.10^{j,k}$	NO	14.0	$< 14.0$	$< -5.29$	108 (Kac11)
J1240+0949	1.045	11698	M. Putman	0.49471	$18.99 \pm 0.18^j$	NO	14.5	$< 14.5$	$< -4.19$	
J1236+0600	1.286	11698	M. Putman	0.54102	$19.88 \pm 0.46^j$	NO	15.3	$< 15.3$	$< -4.28$	
Q1241+176	1.273	12466	J. Charlton	0.55048	$> 19.00^l$	YES	14.3	$15.81 \pm 0.17$	$< -2.89$	21 (Kac11)
Q0107-0232	0.728	11585	N. Crighton	0.55733	$19.50 \pm 0.20^m$	YES	14.0	$17.27 \pm 0.30^m$	$-1.93 \pm 0.36^m$	$10^m$
Q1317+227	1.022	11667	C. Churchill	0.66047	$19.65 \pm 0.10^{j,n}$	NO	14.1	$< 14.1$	$< -5.25$	104 (Kac11)

Notes – <sup>1</sup> $H_2$  detection sensitivity of the spectrum at  $3\sigma$  level. <sup>2</sup> $H_2$  column density when detected, else a  $3\sigma$  upper limit is given. <sup>3</sup>Molecular mass fraction. <sup>4</sup>Impact parameter of the nearest possible host-galaxy candidate when available. References for  $\rho$ : Pet96–Petitjean et al. (1996); Wer13–Werk et al. (2013); Kac11–Kacprzak et al. (2011) <sup>a</sup>From Tripp et al. (2005), a  $3\sigma$  upper limit on  $N(\text{H}_2)$  is obtained from FUSE spectrum. <sup>b</sup>From Meiring et al. (2011). <sup>c</sup>From Srianand et al. (2014). <sup>d</sup> $\log N(\text{H I}) = 19.81 \pm 0.04$  (Lanzetta et al. 1997, using low resolution data). <sup>e</sup>From Oliveira et al. (2014). <sup>f</sup>From Werk et al. (2014). <sup>g</sup>From Battisti et al. (2012). <sup>h</sup> $\log N(\text{H I}) = 18.87 \pm 0.03$  (Tejos et al. 2014). <sup>i</sup> $\log N(\text{H I}) = 19.45^{+0.02}_{-0.03}$  (Rao et al. 2006, using low resolution data). <sup>j</sup> $N(\text{H I})$  is estimated from Voigt profile fitting of higher order Lyman series lines with minimum number of components. Therefore,  $N(\text{H I})$  value should be taken with caution. <sup>k</sup> $\log N(\text{H I}) = 18.65 \pm 0.02$  (Rao et al. 2006, using low resolution data). <sup>l</sup> $N(\text{H I})$  is not well constrained from the COS spectrum due to blend, so we adopt a conservative lower limit;  $\log N(\text{H I}) = 18.90^{+0.07}_{-0.09}$  (Rao et al. 2006, using low resolution data). <sup>m</sup>From Crighton et al. (2013). <sup>n</sup> $\log N(\text{H I}) = 18.57 \pm 0.02$  (Rao et al. 2006, using low resolution data).

**Table 2.** Low- $z$  DLAs/sub-DLAs for which  $H_2$  information is not available.

QSO	PID	PI	$z_{\text{abs}}$	$\log N(\text{H I})$
J1407+5507	12486	D. Bowen	$0.00474^a$	$19.75 \pm 0.05$
J1415+1634	12486	D. Bowen	$0.00775^a$	$19.70 \pm 0.10$
J0930+2848	12603	T. Heckman	$0.02264^a$	$20.71 \pm 0.15$
J1512+0128	12603	T. Heckman	$0.02948^a$	$20.27 \pm 0.15$
J1009+0713	11598	J. Tumlinson	$0.11400^b$	$20.68 \pm 0.10^d$
Q1659+373	12593	D. Nestor	$0.19983^c$	$19.37 \pm 0.20$

Notes – <sup>a</sup>No  $H_2$  coverage. <sup>b</sup>The wavelengths of  $H_2$  transitions are covered but there is no flux below  $\lambda 1241 \text{ \AA}$  due to the complete Lyman limit break from  $z_{\text{abs}} = 0.35590$  system. <sup>c</sup>Only G160M spectrum is available in which  $H_2$  transitions are not covered. <sup>d</sup>From Meiring et al. (2011).

molecular hydrogen. Numerous absorption lines from different rotational levels (starting from  $J = 0$ ) have been searched one-by-one. In total we have found 10 systems where  $H_2$  absorption lines are detected. Three of these 10 systems, i.e.  $z_{\text{abs}} = 0.55733$  towards Q 0107–0232, (Crighton et al. 2013);  $z_{\text{abs}} = 0.18562$  towards B 0120–28, (Oliveira et al. 2014); and  $z_{\text{abs}} = 0.09630$  towards J 1619+3342, (Srianand et al. 2014) were known to have  $H_2$  before. Here we report seven new  $H_2$  detections. All the low- $z$  systems with detected  $H_2$  are listed in Table 3.

For each of the seven cases with new  $H_2$  detections, we choose a set of clean (free from severe blend)  $H_2$  lines from different  $J$  levels for Voigt profile fitting. We fit all the clean lines simultaneously by keeping the Doppler-parameter ( $b$ ) tied. In addition, we constrain the column density to be same for all the transitions from a given  $J$  level and allow it to be different for different  $J$  levels since different molecules are in different rotational states. The COS wavelength calibration is known to have uncertainties at the level of  $10 - 15 \text{ km s}^{-1}$  (Savage et al. 2011; Meiring et al. 2013). Therefore, we did allow the redshift of individual transitions to be different. In majority of the cases lines are aligned within  $\pm 5 \text{ km s}^{-1}$ . However, occasionally, the velocity offset can be up to  $20 \text{ km s}^{-1}$ . Such extreme offsets are noticed only when the lines fall at the edge of the spectra. As an example, in Fig. 2 we show our  $H_2$  fits for the  $z_{\text{abs}} = 0.24788$  system towards J 0925+4004. All the  $H_2$  lines, from different  $J$  levels, that are used for fitting are shown in the plot. Voigt profile fits to  $H_2$  absorption from all other newly reported systems are shown in Appendix-C. The line spread function (LSF) of the COS spectrograph is not a Gaussian. A characterization of the non-Gaussian LSF for COS can be found in Ghavamian et al. (2009) and Kriss (2011). For our Voigt profile fit analysis we adopt the Kriss (2011) LSF. Interpolated LSFs at the line center were con-

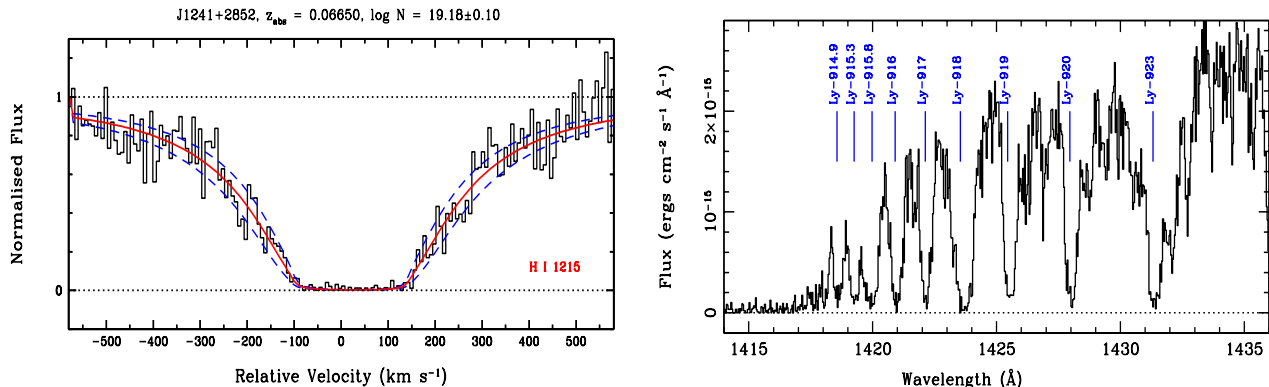


**Figure 1.** Left: Sub-damped Ly $\alpha$  absorption from the  $z_{\text{abs}} = 0.06650$  towards J 1241+2852 system. The solid (red) and dashed (blue) curves represent best fitting Voigt profile to the data (black histogram) and its  $1\sigma$  uncertainty, respectively. Fits for other systems are shown in Appendix-A & B. Right: Strong Lyman limit break from the  $z_{\text{abs}} = 0.55048$  towards Q 1241+176 system. The Ly $\alpha$  is not covered in COS whereas the Ly $\beta$  falls in the gap of the existing spectrum. Both the systems show H $_2$  absorption.

involved with the model Voigt profile while fitting an absorption line using the VPFIT<sup>2</sup> software. Table 3 summarizes the H $_2$  fit parameters derived from the Voigt profile analysis.

All the newly reported H $_2$  systems, except one, are fitted with a single component Voigt profile (see column 2 of Table 3). Apart from the strongest component at 0 km s<sup>-1</sup>, the  $z_{\text{abs}} = 0.10115$  towards Q 0439–433 system shows an additional weak, tentative component at  $-65$  km s<sup>-1</sup>. In general, the Doppler parameters ( $b$ ) obtained in our single component Voigt profile fit, as listed in column 8 of Table 3, are slightly higher than what is typically measured in high- $z$  DLAs. This could indicate the presence of multiple narrow components. Indeed, in cases where we have access to high resolution optical spectra (e.g.  $z_{\text{abs}} = 0.10115$  system towards Q 0439–433), the Na I and Ca II absorption lines show multiple narrow components. However, from high- $z$  H $_2$  systems studied with high resolution, it is known that all the metal components need not produce H $_2$  absorption and observed H $_2$  need not necessarily be associated with the strongest metal absorption (see e.g. Rodríguez et al. 2006). Additionally, because of the wavelength scale uncertainty and relatively lower spectral resolution of COS we do not try to fit H $_2$  lines with multiple components with  $b$ -parameters much less than the spectral resolution. This could lead to underestimation of  $N(\text{H}_2)$  measurements and associated errors.

In the case of non-detections we estimate  $3\sigma$  upper limits on  $N(\text{H}_2)$ , based on the observed error in the continuum, using the following steps: (a) First we look for all the uncontaminated H $_2$  transitions from  $J = 0$  and  $J = 1$  rotational levels that are covered in a spectrum. (b) We derive upper limits on  $N(\text{H}_2)$  for each of those transitions using the prescription by Hellsten et al. (1998), assuming a  $b$ -parameter of 10 km s<sup>-1</sup> (close to the median  $b(\text{H}_2)$  in our sample) for the unresolved H $_2$  line. (c) We adopt the lowest H $_2$  column densities we get for  $J = 0$  and  $J = 1$  levels. The lowest column densities usually come from the transitions with the large  $f\lambda$  values. (d) Finally, we sum the  $N(\text{H}_2)$  limits that we get from  $J = 0$  and  $J = 1$  levels. The estimated upper limits are given in column 9 of Table 1. Note that different spectra in our sample have different SNR and different H $_2$  transitions, depending upon

the absorption redshift, are used to estimate the limits which leads to a wide range in the  $N(\text{H}_2)$  upper limits.

In column 8 of Table 1 we present the H $_2$  detection sensitivity, for each spectrum in our sample, at  $3\sigma$  level. For the systems in which H $_2$  is not detected, the H $_2$  detection sensitivity is the same as the  $3\sigma$  upper limits on  $N(\text{H}_2)$  presented in column 9 of Table 1. For the systems with H $_2$  detections, we estimate  $3\sigma$  upper limits on  $N(\text{H}_2)$ , as described above, from the SNR in the unabsorbed pixels near to the absorption. About half of the spectra in the core sample are sensitive down to  $\log N(\text{H}_2) = 14.4$ , which we denote as the “median sensitivity” limit for our sample.

## 4 ANALYSIS

### 4.1 Incidence/Detection Rate

As mentioned before, there are a total of 27 systems (5 DLAs and 22 sub-DLAs) in our core sample for which the COS spectra cover the expected wavelength range of H $_2$  transitions. Ten out of these 27 systems show absorption lines from molecular hydrogen. Only three of these systems are DLAs and the remaining ones are sub-DLAs. The majority of these systems show H $_2$  absorption from  $J \leq 3$  rotational levels. None of them show higher (i.e.  $J \geq 4$ ) rotational level transitions. The  $z_{\text{abs}} = 0.22711$  system towards J 1342–0053 is detected via  $J = 1$  level transitions alone. Furthermore, for two other systems, i.e.  $z_{\text{abs}} = 0.06650$  towards J 1241+2852 and  $z_{\text{abs}} = 0.16375$  towards Q 0850+440, we do not detect any  $J = 3$  level transitions. Note that Oliveira et al. (2014) did not report any  $J \geq 2$  transitions for the  $z_{\text{abs}} = 0.18495$  H $_2$  component towards B 0120–28. We have verified that  $J \geq 2$  transitions in this component are not detected.

At high redshift ( $1.8 < z_{\text{abs}} < 4.2$ ) Noterdaeme et al. (2008a, hereafter N08) have conducted a survey of molecular hydrogen in DLAs and strong sub-DLAs (with  $\log N(\text{H I}) > 20.0$ ) using high resolution spectra obtained with the Very Large Telescope (VLT) Ultraviolet and Visual Echelle Spectrograph (UVES). The spectral resolution ( $R \sim 45,000$ ) and the typical SNR of their optical spectra are higher than our present survey. They have found only 13 systems with H $_2$  detections in a sample of 77 DLAs/sub-DLAs. Therefore, it appears that the H $_2$  detection is much more frequent at low- $z$  compared to high- $z$ . We quantify this in Fig. 3, where

<sup>2</sup> <http://www.ast.cam.ac.uk/rfc/vpfit.html>

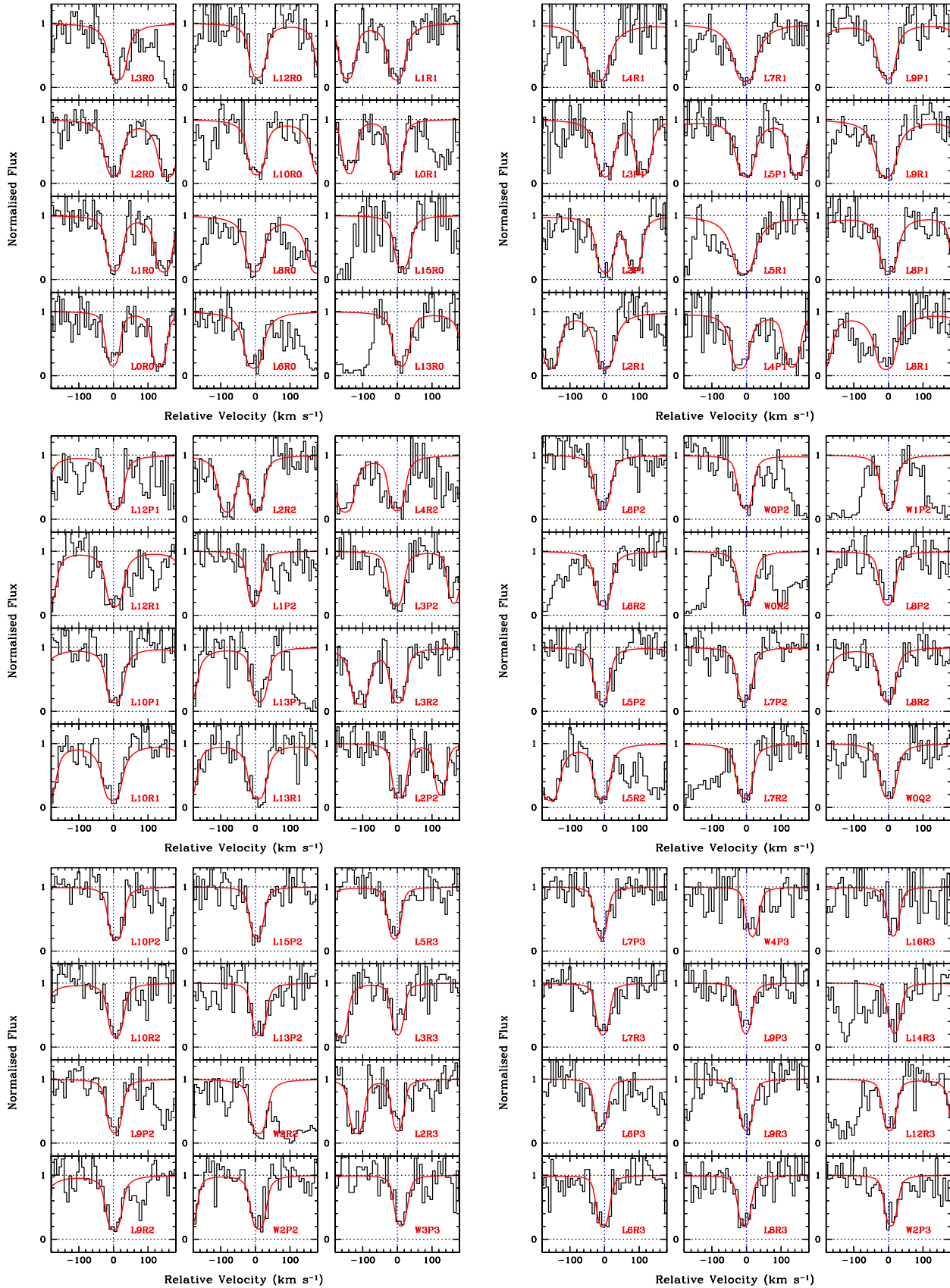


**Figure 2.** Numerous molecular hydrogen absorption lines from different  $J$  levels from the  $z_{\text{abs}} = 0.24788$  towards J 0925+4004 system. The (red) smooth curves are the best fitting Voigt profiles to the data plotted in black histogram.

**Table 3.** Voigt profile fit parameters and other observables for the systems in which H<sub>2</sub> is detected.

QSO	$z_{\text{abs}}$	$\log N(\text{H}_2) \text{ (cm}^{-2}\text{)}$					$b(\text{H}_2)$ (km s <sup>-1</sup> )	$T_{01}$ (K)	$T_{02}$ (K)	$T_{13}$ (K)	$\log Z/Z_{\odot}$
		$J=0$	$J=1$	$J=2$	$J=3$	$J=4$					
(1)	(2)	(3)	(4)	(5)	(6)	(7)	(8)	(9)	(10)	(11)	(12)
J1241+2852	0.06650	15.72±0.08	16.30±0.06	15.45±0.08	< 14.8 <sup>1</sup>	< 14.7 <sup>1</sup>	17.1±1.1	197	229	...	-0.62±0.13 <sup>a</sup>
J1619+3342 <sup>b</sup>	0.09630	18.17±0.04	18.36±0.04	15.97±0.25	15.27±0.29	< 14.1 <sup>1</sup>	4.1±0.4	97	77	107	-0.62±0.13 <sup>f</sup>
Q0439-433	0.10091	14.67±0.05	15.21±0.02	14.91±0.04	14.52±0.07	< 14.1 <sup>1</sup>	32.7±2.6	178	484	350	+0.32±0.14 <sup>a</sup>
	0.10115	15.98±0.06	16.38±0.05	15.70±0.04	15.56±0.04	< 14.1 <sup>1</sup>	12.0±0.5	133	227	311	
Q0850+440	0.16375	14.40±0.03	14.83±0.02	14.33±0.06	< 13.7 <sup>1</sup>	< 13.6 <sup>1</sup>	11.9±0.8	141	289	...	< -1.36 <sup>c</sup>
B0120-28 <sup>d</sup>	0.18495	16.14±0.14	17.23±0.08	< 14.2 <sup>1</sup>	< 14.5 <sup>1</sup>	< 13.8 <sup>1</sup>	...	...	...	...	-1.19±0.21
	0.18524	16.80±0.13	17.45±0.08	14.55 <sup>+0.16</sup> <sub>-0.08</sub>	14.21±0.10	< 13.5 <sup>1</sup>	...	243	75	103	
	0.18550	16.81 <sup>+0.87</sup> <sub>-0.22</sub>	18.91±0.07	18.32±0.05	17.73±0.05	< 13.9 <sup>1</sup>	...	87	...	239	
	0.18568	19.72±0.02	19.53±0.03	18.40±0.04	17.60±0.05	< 13.8 <sup>1</sup>	...	65	110	161	
J1342-0053	0.22711	< 13.4 <sup>1</sup>	14.63±0.06	< 13.6 <sup>1</sup>	< 14.0 <sup>1</sup>	< 14.1 <sup>1</sup>	10.1±2.3	...	...	...	-0.40 <sup>e</sup>
J0925+4004	0.24788	18.15±0.08	18.63±0.04	17.90±0.10	16.83±0.15	< 14.3 <sup>1</sup>	8.4±0.5	156	234	171	-0.29±0.17 <sup>f</sup>
J1616+4154	0.32110	18.95±0.02	18.93±0.02	17.83±0.09	16.99±0.12	< 14.0 <sup>1</sup>	6.9±0.5	76	122	160	-0.38±0.23 <sup>f</sup>
Q1241+176	0.55048	15.35±0.13	15.42±0.06	14.95±0.05	14.80±0.08	< 14.0 <sup>1</sup>	7.8±0.4	83	202	375	< +0.18 <sup>a</sup>
Q0107-0232 <sup>g</sup>	0.55715	16.17±0.25	17.05±0.28	16.19±0.19	15.77±0.12	< 14.0 <sup>1</sup>	6.7±0.6	997	327	225	-0.72±0.32
	0.55729	15.63±0.39	16.42±0.40	15.65±0.25	15.47±0.18	< 14.0 <sup>1</sup>	4.3±0.7	450	327	281	

Notes – <sup>1</sup>Not detected, a formal  $3\sigma$  upper limit is given. <sup>2</sup>Not reported by (Oliveira et al. 2014). <sup>3</sup>Temperature is undefined. <sup>a</sup>Average metallicities ([S/H] or [Si/H]) from this work without ionization correction. <sup>b</sup>All values are taken from Srianand et al. (2014). <sup>c</sup>From Lanzetta et al. (1997). <sup>d</sup>All values are taken from Oliveira et al. (2014). <sup>e</sup>From Werk et al. (2013). <sup>f</sup>From Battisti et al. (2012). <sup>g</sup>All values are taken from Crighton et al. (2013) except the excitation temperatures.

we have compared the H<sub>2</sub> incidence rates in high and low redshift samples for different  $N(\text{H}_2)$  threshold values. In order to estimate incidence rate for a given threshold value, we use *only* spectra that are sensitive to detect H<sub>2</sub> down to the threshold  $N(\text{H}_2)$ . The incidence rate is then derived by taking the ratio of number of systems in which H<sub>2</sub> is detected with  $N(\text{H}_2)$  higher than the threshold value to the total number of systems. As mentioned before, the “median sensitivity” of our sample is  $\log N(\text{H}_2) = 14.4$  whereas for the high- $z$  sample it is  $\log N(\text{H}_2) = 14.2$ . Note that for the 13 high- $z$  H<sub>2</sub> systems of N08’s sample we have derived the spectral sensitivity for H<sub>2</sub> detection at  $3\sigma$  level in the same fashion as described in the previous section.

It is apparent from Fig. 3 that the H<sub>2</sub> incidence rate is higher at low- $z$  for the whole range of  $N(\text{H}_2)$  threshold values up to  $\log N(\text{H}_2) = 16.5$ . The difference is increasingly higher for lower  $N(\text{H}_2)$  thresholds. For a threshold column density of  $\log N(\text{H}_2) = 14.4$ , the H<sub>2</sub> incidence rate at low- $z$  is  $50^{+25}_{-12}$  percent, whereas it is only  $18^{+8}_{-4}$  percent at high- $z$ . Therefore, the H<sub>2</sub> incidence rate is  $\gtrsim 2$  times higher at low- $z$  with a  $\sim 2\sigma$  confidence. Recently, in a blind survey for H<sub>2</sub> in DLAs, observed with mostly poor spectral resolution ( $\sim 71 \text{ km s}^{-1}$ ) data, Jorgenson et al. (2014) have found a paucity of strong H<sub>2</sub> systems (e.g.  $\sim 1$  percent detection rate for  $\log N(\text{H}_2) > 18$ ). For a  $N(\text{H}_2)$  threshold as high as  $10^{18} \text{ cm}^{-2}$ , the H<sub>2</sub> detection rate in our low- $z$  sample (i.e.  $15^{+12}_{-4}$  percent) is higher than that found by Jorgenson et al. (2014) but consistent with the sample of N08 (i.e.  $10^{+5}_{-3}$  percent). In passing, we wish to point out that using high redshift ( $z > 2$ ) QSO spectra from the Sloan Digital Sky Survey (SDSS), Balashev et al. (2014) have found an upper limit in detection rate of  $\sim 7$  percent for strong H<sub>2</sub> systems with  $\log N(\text{H}_2) > 19.0$ . For our sample, we find a detection rate of  $7^{+10}_{-2}$  percent for a similar  $N(\text{H}_2)$  threshold.

## 4.2 Column density distributions

The total H<sub>2</sub> column density of a given system with detected H<sub>2</sub>, as listed in column 9 of Table 1, is derived by summing the column densities measured in different  $J$  levels as listed in columns

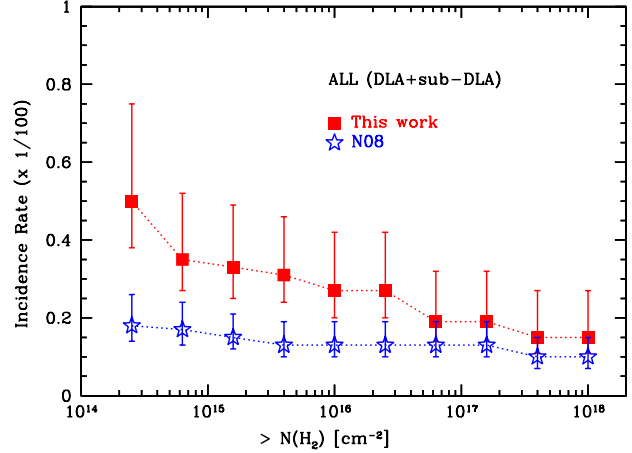


**Figure 3.** Incidence rates of molecular hydrogen for our low- $z$  sample (red squares) and the high- $z$  sample of N08 (blue stars) against different threshold  $N(\text{H}_2)$  values. Errorbars represent Gaussian  $1\sigma$  confidence intervals computed using tables of Gehrels (1986) assuming a Poisson distribution.

3, 4, 5, and 6 of Table 3. For multicomponent systems, component column densities are further summed up to get the total  $N(\text{H}_2)$ . The total H<sub>2</sub> column density distribution for our low- $z$  sample is compared with that of the high- $z$  sample of N08 in the left panel of Fig. 4. We do not find any significant difference between them. A two-sided Kolmogorov-Smirnov (KS) test suggests that the maximum deviation between the two cumulative distribution functions is  $D_{\text{KS}} = 0.37$  with a probability of  $P_{\text{KS}} = 0.34^3$ .

In the right panel of Fig. 4 the H I column density distributions of our core sample (total 27 systems) and the sample of N08 (total 77 systems) are shown. It is clearly evident that the two distributions are significantly different. A two-sided KS-test also supports

<sup>3</sup>  $P_{\text{KS}}$  is the probability of finding this  $D_{\text{KS}}$  value or lower by chance.

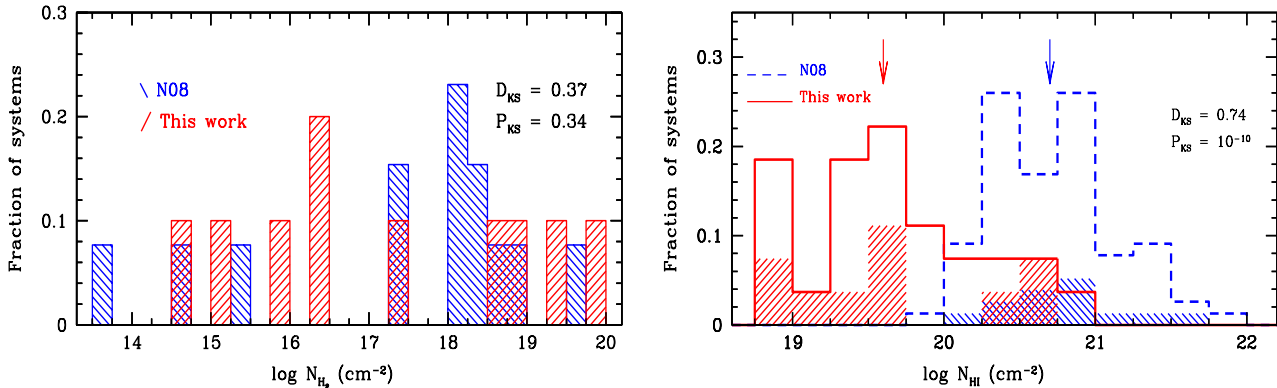


**Figure 4.** Left: The  $N(H_2)$  distributions for the low- $z$  sample (red  $45^\circ$  hatched histogram) and the high- $z$  sample of N08 (blue  $135^\circ$  hatched histogram). Right: The  $N(HI)$  distributions of our core sample (red solid histogram) and the sample of N08 (blue dashed histogram). The arrows mark the median values. The (red)  $45^\circ$  and (blue)  $135^\circ$  hatched histograms show the  $N(HI)$  distributions for the systems with  $H_2$  detections in low- and high- $z$  samples respectively.

this with a  $D_{KS} = 0.74$  and a  $P_{KS} \sim 10^{-10}$ . The median value of  $\log N(HI) = 19.6$  for our low- $z$  sample is an order of magnitude lower than that of the high- $z$  sample. In the low- $z$  sample only 7 systems show  $\log N(HI) > 20.0$ , whereas all 77 high- $z$  systems have  $\log N(HI) > 20.0$ . Therefore, in order to make a more realistic comparison it is important to increase the sample sizes of the sub-DLAs at high- $z$  and the DLAs at low- $z$ .

The hatched histograms in the figure show the  $N(HI)$  distributions for the systems in which  $H_2$  is detected. It is interesting to note that there is no preference for molecular hydrogen to originate from higher (or lower)  $N(HI)$  systems. A two-sided KS-test suggests that the  $N(HI)$  distributions for systems with and without  $H_2$  detections are very similar (e.g.  $D_{KS} = 0.18$  and  $P_{KS} = 0.97$ ). N08 have found the same for their high- $z$  sample. As noted earlier, a significant fraction (i.e. 7 out of 10) of low- $z$   $H_2$  systems show  $\log N(HI) < 20$ . Detection of  $H_2$  at lower  $N(HI)$  and the enhanced incidence rate could possibly suggest that the low- $z$  sub-DLAs have (a) higher metallicities and/or dust, (b) higher densities, and/or (c) weaker radiation field. We discuss these issues in Section 5.

### 4.3 The molecular mass fraction, $f_{H_2}$

The molecular mass fraction,  $f_{H_2}$ , of a DLA/sub-DLA system is defined as:

$$f_{H_2} = \frac{2N(H_2)}{N(HI) + 2N(H_2)}. \quad (1)$$

At the median  $N(HI)$ , the ‘‘median sensitivity’’ limit of our survey (i.e.  $\log N(H_2) = 14.4$ ) corresponds to a  $f_{H_2} = 10^{-4.9}$ . We, therefore, denote this as our median  $f_{H_2}$  sensitivity limit. In four different panels of Fig. 5 we have plotted  $f_{H_2}$  against total hydrogen column density,  $N_H = N(HI) + 2N(H_2)$ . We note that for sub-DLAs this is a lower limit in  $N_H$  as we are ignoring the ionized fraction.

In panel-(A) we have compared low- and high- $z$  samples in the  $f_{H_2} - N_H$  plane. As already noted, the low- $z$  systems have lower  $N_H$  values (always  $N_H < 10^{20.7} \text{ cm}^{-2}$ ) compared to high- $z$ . There are a few detections with very low molecular fractions ( $f_{H_2} \lesssim 10^{-4.9}$ ) in the high- $z$  sample. Such low  $f_{H_2}$  systems are not present in our sample. We perform a two-sample survival analysis, including censored data points (upper limits), in order to investigate if  $f_{H_2}$  distributions at high- $z$  and low- $z$  are drawn from the same

**Table 4.** Results of log-rank tests between  $f_{H_2}$  distributions.

Sample-1	Sample-2	$> \log f_{H_2}^a$	$\chi^2{}^{2b}$	$P_{\log\text{-rank}}^c$
Low- $z$	High- $z$	-8.0	6.2	0.013
Low- $z$	High- $z$	-4.9	0.6	0.444
Low- $z$	ISM (Halo)	-4.9	6.7	0.009
Low- $z$	ISM (Disk)	-4.9	14.8	$10^{-4}$
Low- $z$	SMC	-4.9	15.2	$10^{-4}$
Low- $z$	LMC	-4.9	15.2	$10^{-4}$

Notes – <sup>a</sup>Threshold  $\log f_{H_2}$ . <sup>b</sup>The  $\chi^2$  statistic for a test of equality. <sup>c</sup>Probability of rejecting null hypothesis by chance.

parent populations<sup>4</sup>. The log-rank test rejects the null hypothesis with a confidence of 98.7% (see Table 4), suggesting only a mild difference. When we consider only systems with  $\log f_{H_2} > -4.9$ , the log-rank test rejects the null hypothesis with a confidence of only 56%, implying a lack of any statistically significant difference in the  $f_{H_2}$  distribution. We point out that the mild difference suggested by the log-rank test for the entire sample is merely due to the fact that the  $H_2$  detection rate is considerably higher at low- $z$  than at high- $z$ .

In panel-(B) of Fig. 5 we compare our sample with that of the Savage et al. (1977, i.e. the Galactic disk) and Gillmon et al. (2006, i.e. the Galactic halo) samples. The Galactic samples clearly show a transition near  $\log N_H = 20.7$ , above which all systems have molecular fraction  $\log f_{H_2} \gtrsim -1$ . This transition, leading to a bimodality in the  $f_{H_2}$  distribution, is generally identified as the threshold above which the  $H_2$  molecule gets completely self-shielded from interstellar radiation (Savage et al. 1977). Such a transition is not apparent in the low- $z$  and/or high- $z$  sample. This is what is expected since they trace a wide variety of environments (e.g. different metallicities, dust depletion, radiation field etc.) unlike the sightlines passing through a single galaxy. A log-rank test of the  $f_{H_2}$  distributions between our low- $z$  sample and the Galactic disk sample of Savage et al. (1977), for systems with  $\log f_{H_2} > -4.9$ , indicates that they are significantly different (e.g. rejects the null-hypothesis with a confidence of  $> 99.99\%$ ). This is also true when we compare low- $z$   $f_{H_2}$  distribution with that of

<sup>4</sup> We have used the ‘‘survdiff’’ function under the ‘‘survival’’ package in R (<http://www.r-project.org/>).

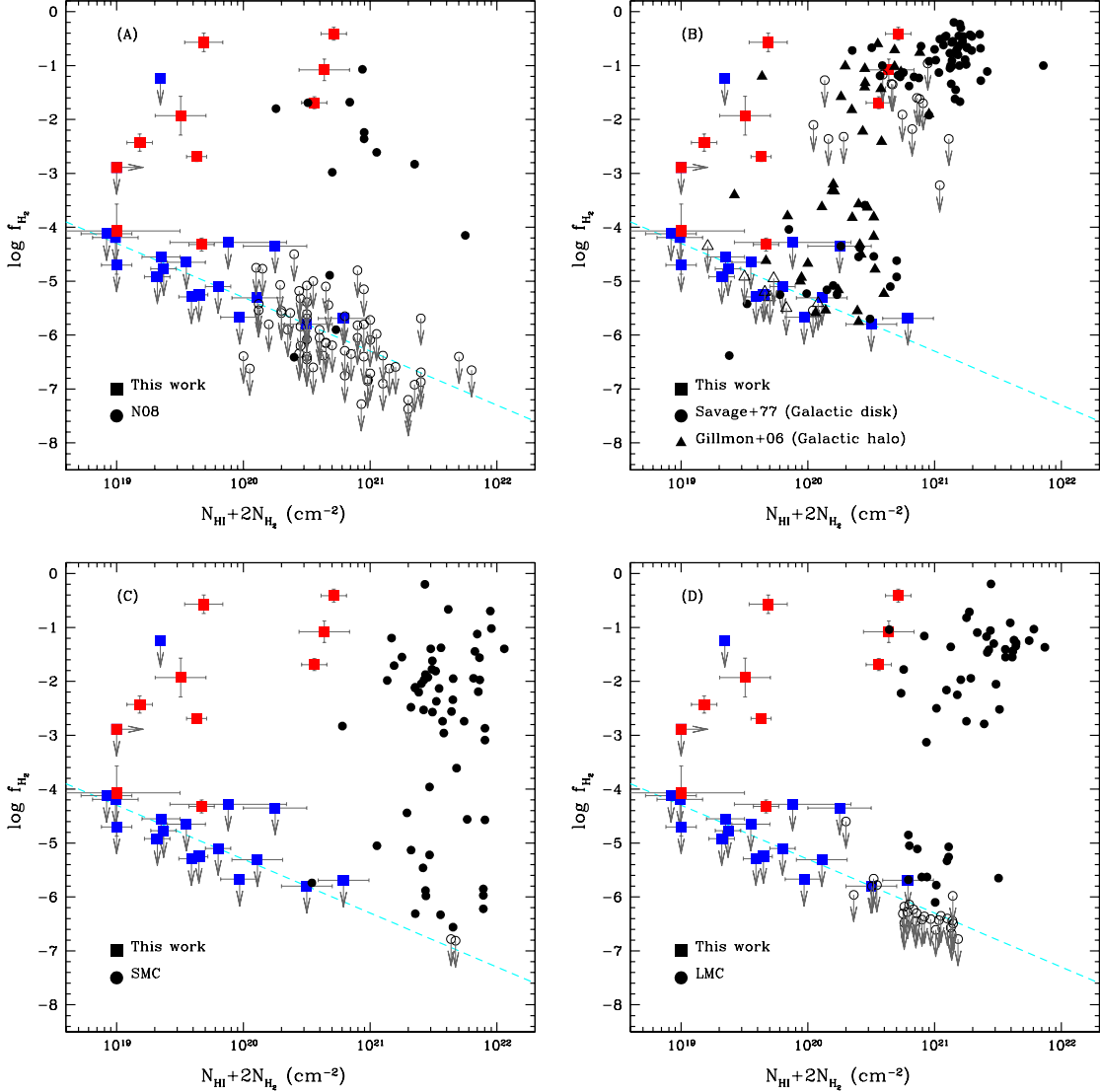


**Figure 5.** The molecular mass fraction against the total hydrogen (neutral atomic + molecular) column density,  $N(\text{HI} + \text{H}_2)$ . In each panel squares represent our low- $z$  sample (with red squares corresponding to  $\text{H}_2$  detections), whereas circles/triangles represent other samples as indicated in the panel (with filled ones corresponding to  $\text{H}_2$  detections). The dashed line corresponds to our “median sensitivity” limit i.e.  $\log N(\text{H}_2) = 14.4$ .

the Galactic halo (Gillmon et al. 2006) sample, albeit with slightly lower confidence (e.g. 99.1% confidence, see Table 4).

In panel-(C) and (D) of Fig. 5, the low- $z$  sample is compared with the SMC and LMC, respectively. Here we have taken both Tumlinson et al. (2002) and Welty et al. (2012) measurements into account. For lines of sight that are common in both the studies, we used updated measurements from Welty et al. (2012). It is clear that our low- $z$  sample and the Magellanic Cloud systems have only marginal overlap, with the latter having systematically higher  $N_{\text{H}}$  values. Unlike the Galactic lines of sight, the transition in  $f_{\text{H}_2}$  due to self-shielding is not very prominent for SMC systems. LMC systems, however, show such transition albeit at higher  $N_{\text{H}}$  values (i.e. at  $\log N_{\text{H}} = 21.3$ ). A log-rank test of  $f_{\text{H}_2}$  distributions between our low- $z$  sample and the SMC/LMC, for systems with  $\log f_{\text{H}_2} > -4.9$ , suggests that they are drawn from significantly different parent populations (e.g. rejects the null-hypothesis with a probability of  $> 99.99\%$ , see Table 4).

It is clearly evident from Fig. 5 that our low- $z$   $\text{H}_2$  systems predominantly populate the upper-left corner of the  $f_{\text{H}_2} - N_{\text{H}}$  plane (i.e.  $f_{\text{H}_2} \gtrsim -4.5$  and  $\log N_{\text{H}} \lesssim 20.7$ ). This is a unique region in the parameter-space. Only one of the Magellanic Cloud systems, three high- $z$  systems and a few (8/72) Galactic disk systems, with detected  $\text{H}_2$ , fall in this region. The key reason for this observation is that our low- $z$  sample is primarily comprised of sub-DLAs. It is interesting to note that even with systematically lower  $N_{\text{H}}$  values, many low- $z$  systems show a considerably large molecular fraction. We discuss possible reasons for that in view of simple photoionization models in Section 5.3. The Galactic disk/Magellanic Clouds/high- $z$  samples are primarily composed of DLAs with  $N_{\text{H}} > 10^{21} \text{ cm}^{-2}$ . Therefore, we point out that for a realistic comparison of  $f_{\text{H}_2}$  distributions, as presented in Table 4, more observations of molecular hydrogen in DLAs at low- $z$  are extremely important. Additionally, more observations of  $\text{H}_2$  in sub-DLAs at high- $z$  are crucial for comparing with our current low- $z$



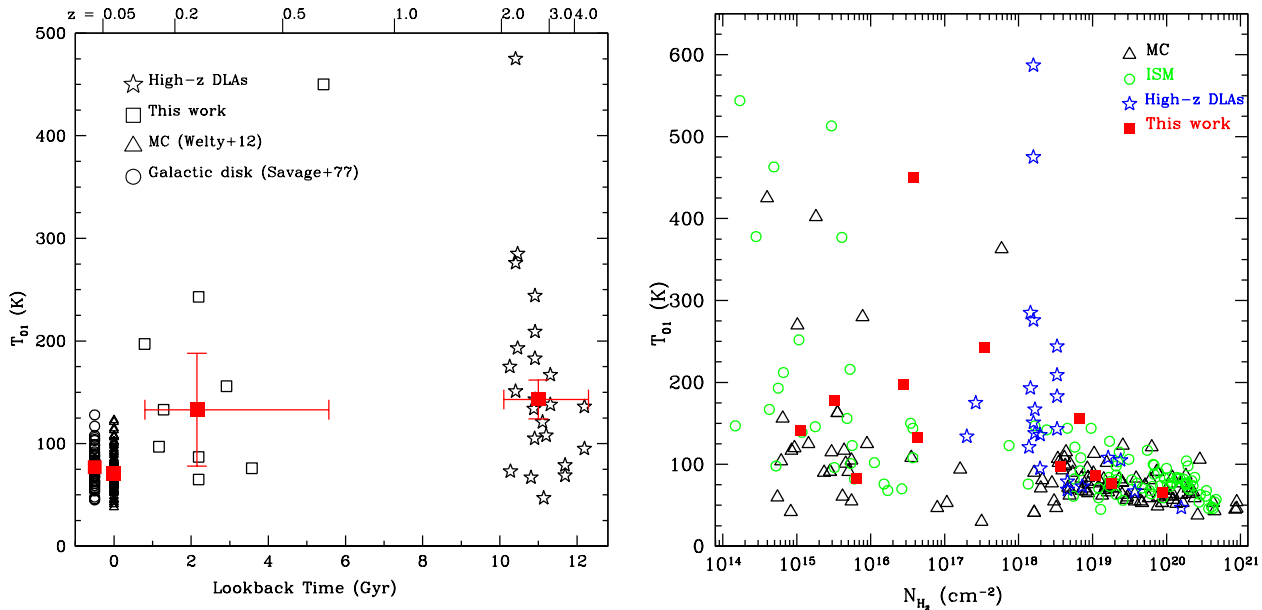


**Figure 6.** Left: Cosmic evolution of the rotational excitation temperature,  $T_{01}$ . Only components with total  $\log N(\text{H}_2) > 16.5$  are used. The (red) filled squares represent the median values in each sample. Errorbars along y-axis are the  $1\sigma$  Gaussian errors on the median value computed from bootstrapping. Errorbars along x-axis are just to show the spread in look-back time for high- and low- $z$  samples. The Galactic measurements are shifted to the left for clarity. Here we have excluded the temperature measurements in the  $z_{\text{abs}} = 0.55715$  component towards Q 0107–0232. Right:  $T_{01}$  against  $\text{H}_2$  column density for different samples plotted with different symbols. The (green) open circles (ISM) are from Savage et al. (1977) and Gillmon et al. (2006). The (magenta) open triangles (Magellanic Clouds, MC) are from Tumlinson et al. (2002) and Welty et al. (2012). The (blue) stars are from the “high- $z$  DLAs” as defined in the text. The data points plotted as (red) squares are from this study.

sample. The only possible exception is the Galactic halo sample. We would like to emphasize here that a significantly large fraction (e.g.  $25/40 \sim 63\%$ ) of the Galactic halo systems, in which  $\text{H}_2$  is detected, have  $f_{\text{H}_2}$  and  $N_{\text{H}}$  in the range similar to as seen for our low- $z$  sample. This perhaps indicates that the origin(s) and the physical conditions of molecular gas in low- $z$  DLAs/sub-DLAs are similar to that of the Milky Way halo gas.

#### 4.4 The excitation temperature, $T_{01}$

The rotational excitation temperature,  $T_{01}$ , for  $J = 0$  to  $J = 1$  rotational levels can be expressed as:

$$\frac{N(J=1)}{N(J=0)} = \frac{g_1}{g_0} \exp(-170.5/T_{01}). \quad (2)$$

Here  $g_0$ ,  $g_1$  are the statistical weights for  $J = 0$  and  $J = 1$  rotational levels respectively. When  $\text{H}_2$  is sufficiently self-shielded (e.g.  $\log N(\text{H}_2) > 16.5$ ) from photo-dissociating photons, collisional processes dominate the level populations, then  $T_{01}$  represents the kinetic temperature of the absorbing gas (Snow et al. 2000; Roy et al. 2006). The excitation temperatures ( $T_{01}$ ) measured from  $\text{H}_2$  absorption in our sample are summarized in column 9 of Table 3. The median value of  $T_{01}$  in our sample is  $T_{01} = 133 \pm 75$  K for the  $\text{H}_2$  components with a total  $N(\text{H}_2) > 10^{16.5} \text{ cm}^{-2}$ . The large scatter results from the large  $T_{01}$  value (i.e. 997 K) measured in one of the components in  $z_{\text{abs}} = 0.55733$  towards Q 0107–0232 system. The median value becomes  $T_{01} = 133 \pm 55$  K when we exclude the outlier. Note that the errors in the median  $T_{01}$  values in this work are estimated from bootstrapping unless specified.

In the left panel of Fig. 6 we show the evolution of  $T_{01}$  over the last 12 Gyr of cosmic time. Measurements from

different samples at different cosmic time (or redshift) are shown in different symbols. The local measurements are taken from Savage et al. (1977, the Galactic disk) and Welty et al. (2012, the Magellanic Clouds), whereas the high- $z$  measurements are from Petitjean et al. (2002), Srianand et al. (2005, 2008), Ledoux et al. (2006b), Noterdaeme et al. (2007, 2008a, 2010), and Guimarães et al. (2012). Hereafter, we will refer this ensemble of systems as “high- $z$  DLAs”. The median  $T_{01}$  in our low- $z$  sample (i.e.  $133 \pm 55$  K) is very similar to that of the “high- $z$  DLAs” (i.e.  $143 \pm 19$  K). The local measurements of  $T_{01}$ , i.e.  $77 \pm 02$  K in the Galactic disk,  $115 \pm 13$  K in the Galactic halo, and  $71 \pm 03$  K in the Magellanic Clouds, are slightly lower but roughly consistent with the low- $z$  measurements within the large scatter.

In the right panel of Fig. 6,  $T_{01}$  is plotted against the  $\text{H}_2$  column density for various different samples.  $T_{01}$ , in general, seem to show a large scatter for lower values of  $N(\text{H}_2)$ . On the contrary, for  $\log N(\text{H}_2) > 19.0$  all systems show  $T_{01} < 120$  K, irrespective of which samples they come from. This can be understood in terms of efficient shielding of radiation in higher  $N(\text{H}_2)$  systems. In columns 10 and 11 of Table 3 we present  $T_{02}$  and  $T_{13}$ , respectively, estimated using Eqn. 3 of Srianand et al. (2005). These values are typically higher than the corresponding  $T_{01}$  measurements. Such elevated  $T_{02}$  and/or  $T_{13}$  values compared to  $T_{01}$  have been interpreted as the influence of radiation pumping and/or formation pumping (Tumlinson et al. 2002; Srianand et al. 2005). Higher rotational level (i.e.  $J \geq 4$ ) populations (e.g.  $N_4/N_2$  or  $N_5/N_3$  ratios) are even more sensitive probes of radiation/formation pumping (see e.g. Tumlinson et al. 2002). None of the low- $z$   $\text{H}_2$  systems show detectable absorption from  $J \geq 4$  levels. This clearly suggests that the radiation/formation pumping may not be severe for the  $\text{H}_2$  systems in our sample.

## 5 DISCUSSIONS

### 5.1 Enhanced incidence rate of $\text{H}_2$ at low- $z$

We find that the incidence rate of  $\text{H}_2$  absorption in our low- $z$  sample is generally higher compared to the high- $z$  sample of N08 for different  $N(\text{H}_2)$  threshold values up to  $\log N(\text{H}_2) = 16.5$ . In our sample the  $\text{H}_2$  incidence rate is found to be  $50^{+25}_{-12}$  percent, for systems with  $\log N(\text{H}_2) > 14.4$ , detected in spectra that are sensitive down to  $\log N(\text{H}_2) = 14.4$ . The incidence rate is a factor of  $\gtrsim 2$  higher compared to the high- $z$  sample of N08, in which it is only  $18^{+8}_{-4}$  percent for a similar  $N(\text{H}_2)$  threshold. The occurrence of enhanced  $\text{H}_2$  incidence rate at low- $z$  is unlikely due to sample bias as none of these spectra were obtained in order to study molecular hydrogen. We note that the program ID 12593 (PI: D. Nestor) was proposed to observe low- $z$  DLAs but no  $\text{H}_2$  is detected from that dataset. In addition, program ID 12536 (PI: V. Kulkarni) was proposed to observe low- $z$  sub-DLAs and one of these shows  $\text{H}_2$  absorption. But none of these proposals were focussed on  $\text{H}_2$  that was known beforehand.

The cosmic mean metallicity of DLAs is known to increase with cosmic time (Prochaska et al. 2003; Rafelski et al. 2012). From their best fitting metallicity versus redshift relationship, we expect the metallicity of the low- $z$  DLAs (at  $z \lesssim 0.5$ ) to have  $\sim 0.5$  dex higher metallicity compared to the DLAs in the sample of N08. Moreover, sub-DLAs have higher metallicities than DLAs at any given epoch and show faster metallicity evolution (e.g. Kulkarni et al. 2007; Som et al. 2013). From Fig. 11 of Som et al. (2013) we notice that in the case of sub-DLAs at  $z \lesssim 0.5$ , the enhancement in the  $N(\text{H I})$ -weighted mean metallicity could be as high as 0.7 dex compared to sub-DLAs at  $z \simeq 2.5$ . Both the above mentioned facts suggest that the probability of finding a metal-rich DLA and/or sub-DLA at high- $z$  should be lower than that at low- $z$ . Note that a vast majority (22/27) of our low- $z$  sample are sub-DLAs. In the next section, we demonstrate that the metal-rich DLAs/sub-DLAs are more likely to have molecules (see also Petitjean et al. 2006; Noterdaeme et al. 2008a). This possibly explains the higher incidence rate of molecular hydrogen at low redshift. We plan to investigate this issue in detail in our future work.

### 5.2 Evolution of $f_{\text{H}_2}$

In equilibrium between formation and photo-dissociation, the molecular mass fraction can be written as:

$$f_{\text{H}_2} = \frac{2Rn_{\text{HI}}}{D}, \quad (3)$$

where,  $R$  (in  $\text{cm}^3 \text{s}^{-1}$ ) is the formation rate coefficient and  $D$  (in  $\text{s}^{-1}$ ) is the photo-dissociation rate. In a cold and neutral gas phase,  $\text{H}_2$  formation occurs on the surface of dust grains. Thus,  $R$  is proportional to the dust-to-gas ratio ( $\kappa$ ). Note that  $\kappa$  depends on the metallicity of the gas. The dissociation rate,  $D$ , on the other hand, depends crucially on the ionizing radiation. There are several indications that  $f_{\text{H}_2}$  should increase with cosmic time:

(a) The global star-formation rate density (or luminosity density) of galaxies decreases with time (see e.g. Bouwens et al. 2011). This suggests that if  $\text{H}_2$  systems are related to star forming disks at all epochs, then low- $z$  systems will experience a much weaker ionizing radiation field compared to high- $z$  systems. This will lead to a decrease in the photo-dissociation rate.

(b) The extra-galactic UV background radiation gets fainter by about an order of magnitude at low- $z$  compared to high- $z$  ( $z > 2$ ) as a consequence of the decrease in the global star-formation rate

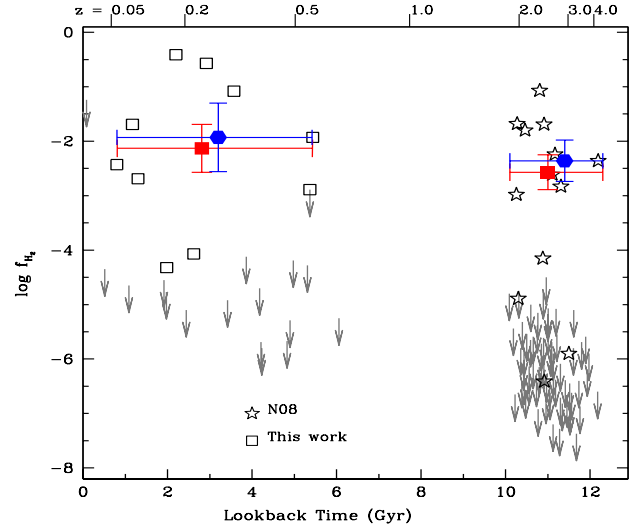


**Figure 7.** Cosmic evolution of the molecular mass fraction. Open squares and open stars represent measurements from our low- $z$  and the high- $z$  sample of N08, respectively. Filled (red) squares and (blue) diamonds, respectively, represent the mean and median of  $\log f_{\text{H}_2}$ , for the systems in which  $\text{H}_2$  is detected with a  $\log f_{\text{H}_2} > -4.9$  in each sample. The errorbars in mean and median  $\log f_{\text{H}_2}$  are computed from bootstrapping. The errorbars along  $x$ -axis are just to show the spread in look-back time for each sample.

density (Haardt & Madau 1996, 2012). This implies that if  $\text{H}_2$  systems are related to halo gas, where extra-galactic UV background radiation dominates over the radiation field of the host-galaxy, then again low- $z$  systems will experience a much weaker ionizing radiation compared to high- $z$  systems.

(c) An increase in the cosmic mean metallicity with time (Prochaska et al. 2003; Rafelski et al. 2012), suggests that the  $\text{H}_2$  formation rate will be higher at low- $z$ , leading to an increase in  $f_{\text{H}_2}$ . Furthermore, we note that sub-DLAs tend to show higher metallicities and faster metallicity evolution compared to DLAs (Kulkarni et al. 2007; Som et al. 2013). Since our low- $z$  sample contains a larger fraction of sub-DLA that are supposed to have higher metallicities, an enhanced  $\text{H}_2$  formation rate in these low- $z$  systems is expected.

In Fig. 7 we show the evolution of  $f_{\text{H}_2}$  over the last 12 Gyr of cosmic time. The high- and low- $z$  samples are presented in open stars and open squares, respectively. Upper limits in both the samples are shown by arrows. The mean and median values of  $\log f_{\text{H}_2}$ , for the systems in which  $\text{H}_2$  is detected with a  $\log f_{\text{H}_2} > -4.9$ , are found to be  $-2.13 \pm 0.44$  and  $-1.93 \pm 0.63$ , respectively. These values are only  $\sim 2.7$  times higher than the corresponding values at high- $z$ . This could result from the fact that the  $N(\text{H}_2)$  distributions at high- and low- $z$  are very similar whereas the low- $z$  systems have systematically lower  $N(\text{H I})$  values. Nevertheless, the mean/median values of  $\log f_{\text{H}_2}$  at high- and low- $z$  are consistent within  $1\sigma$  allowed range.

Finally, we have performed the Kendall's  $\tau$  correlation test including censored data points between absorption redshift and  $\log f_{\text{H}_2}$ <sup>5</sup>. A mild anti-correlation is suggested by the Kendall's  $\tau$  test with a  $\tau = -0.27$  and with a confidence of 99.99 percent, when we consider all the systems from both the high- and the low-

<sup>5</sup> We have used the “*cenken*” function under the “*NADA*” package in R

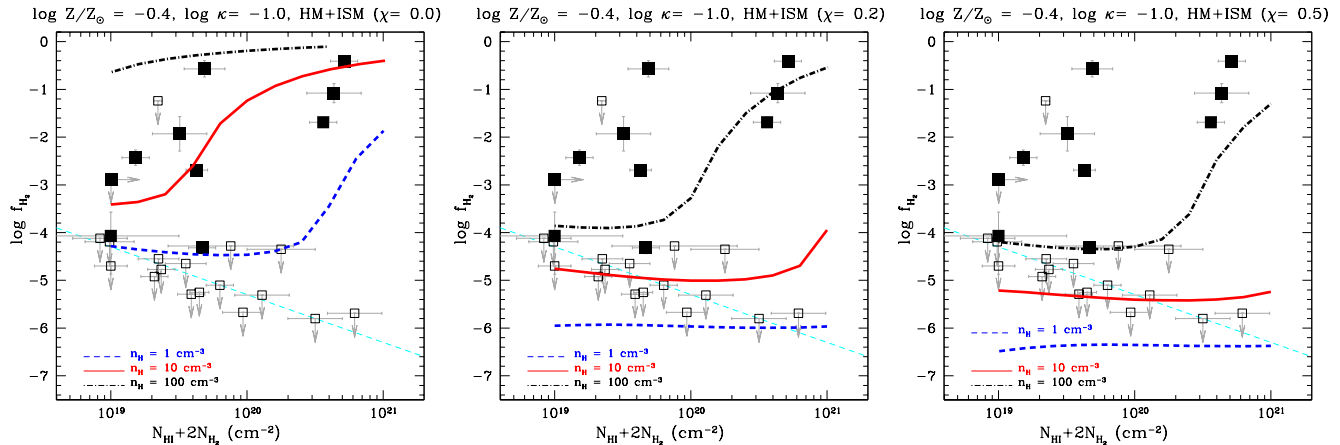


**Figure 8.** The molecular mass fraction against the total hydrogen (atomic+molecular) column density in our sample. The systems in which  $H_2$  is detected are plotted as solid squares. The dashed straight line corresponds to a  $\log N(H_2) = 14.4$ . Results of photoionization model predictions for three representative densities are shown by smooth curves in each panel. Models of three different panels assume three different ionizing radiation (see text). All models assume a metallicity of  $\log Z/Z_\odot = -0.4$  and a dust-to-gas ratio of  $\log \kappa = -1.0$ .

$z$  samples. This mild anti-correlation is essentially the manifestation of the fact that the incidence rate of  $H_2$  is considerably higher at low- $z$ . However, no correlation is found (e.g.  $\tau = -0.08$  with a  $\sim 78$  percent confidence) when we consider only system with  $\log f_{H_2} > -4.9$ .

In a study of about 30 million simulated galaxies in the Millennium simulation (Springel et al. 2005), Obreschcow & Rawlings (2009) have found a strong decrease in  $H_2$  masses,  $\Omega_{H_2}$ , in regular galaxies between  $z = 2$  to 0 (see their Fig. 2). In their pressure-based model, it is assumed that all cold gas resides in a flat symmetric disk with an exponential surface density profile. Therefore, if DLAs/sub-DLAs are truly tracing disks/ISM of typical regular galaxies throughout the cosmic ages then one would expect an evolution in the  $N(H_2)$  distribution. Using a two-sided KS test, we do not find any statistically significant difference in  $N(H_2)$  distributions at high- and low- $z$ , for the systems in which  $H_2$  is detected. This possibly indicates that DLAs/sub-DLAs do not, in general, trace disks and/or the ISM of regular galaxies.

### 5.3 Overall physical conditions

To understand the overall physical conditions in these low- $z$   $H_2$  systems we run grids of photoionization models using CLOUDY (v13.03, last described by Ferland et al. 2013). The models predicted molecular mass fractions as a function of total hydrogen column density (atomic+molecular) are shown in three different panels of Fig. 8. In each panel, models are run for three different densities (i.e.  $n_H = 1, 10, \text{ and } 100 \text{ cm}^{-3}$ ), assuming a metallicity of  $\log Z = -0.4$  (the median value for our sample, see column 12 of Table 3) and a dust-to-gas ratio of  $\log \kappa = -1.0$  (a fiducial value). The ionizing radiation field for the models shown in the left panel is the extra-galactic UV background radiation computed by Haardt & Madau (2001) at  $z = 0.2$ . It is apparent from this panel that the model with  $n_H = 1 \text{ cm}^{-3}$  cannot explain the majority of the systems where  $H_2$  is detected. The model with  $n_H = 10 \text{ cm}^{-3}$  seems to be a better choice. Now when we add the mean UV radiation field as seen in the Galactic ISM (Habing 1968) but scaled by a factor of  $\chi = 0.2$ , the model with  $n_H = 10 \text{ cm}^{-3}$  clearly does not work (see middle panel). A particle density of  $n_H = 100 \text{ cm}^{-3}$  is preferred instead. If we further increase the contribution of

mean Galactic radiation field by increasing the scaling factor to a  $\chi = 0.5$ , even the model with  $n_H = 100 \text{ cm}^{-3}$  fails to reproduce the observed molecular fractions (see right panel).

At high redshift, the density of the  $H_2$  bearing components in DLAs found to be in the range  $10\text{--}200 \text{ cm}^{-3}$  with a radiation field of the order of or slightly higher than the mean UV radiation field in the Galactic ISM (i.e.  $\chi \gtrsim 1.0$ , see Srianand et al. 2005). If the low- $z$   $H_2$  systems originate from a similar density range then the UV radiation field prevailing in these systems has to be much weaker (i.e.  $\chi \lesssim 0.5$ ). Therefore, we speculate that the low- $z$   $H_2$  systems are possibly not related to star-forming disks, but trace regions that are farther away from the luminous part of a galaxy. The large impact parameters of possible host-galaxy candidates, as discussed below, further promote such an idea.

### 5.4 Connection to galaxies

A search for galaxies responsible for DLA/sub-DLA absorption at low redshift ( $0.1 \lesssim z \lesssim 1$ ) by Rao et al. (2011) has shown that the median impact parameter is  $\sim 17 \text{ kpc}$  for the DLA host-galaxies ( $\sim 35 \text{ kpc}$  for the sub-DLAs). Using H I 21-cm maps of nearby galaxies, Zwaan et al. (2005) have found that the sight-lines with  $\log N(H I) \geq 20.3$  typically occur with an impact parameter of  $\rho < 7 \text{ kpc}$ . The DLA host-galaxies that produce strong  $H_2$  absorption (e.g.  $N(H_2) > 10^{21} \text{ cm}^{-2}$ ) tend to have such low impact parameters (Zwaan & Prochaska 2006). The strong  $H_2$  systems are the potential candidates where CO molecules are most likely to be detected. In fact, using interferometric images of CO emission lines, Young (2002) has found that the molecular gas is distributed in mostly symmetric rotating disks with diameters of  $2\text{--}12 \text{ kpc}$  in nearby elliptical galaxies. Even at high redshift ( $z \sim 2$ ), CO emission lines from sub-millimeter galaxies have been shown to originate in disks (Tacconi et al. 2006). All these suggest that although median impact parameters of DLA/sub-DLA host-galaxies are  $\gtrsim 20 \text{ kpc}$ , molecular gas extends only up to  $\lesssim 10 \text{ kpc}$  along the optical disks of galaxies. Recent simulations also predict this (see e.g. Bekki 2014; Yozin & Bekki 2014).

For eight out of the ten low- $z$   $H_2$  systems, we have host-galaxy information from the literature (see column 11 of Table 1). In Fig. 9 we show the molecular fractions against the impact parameters of

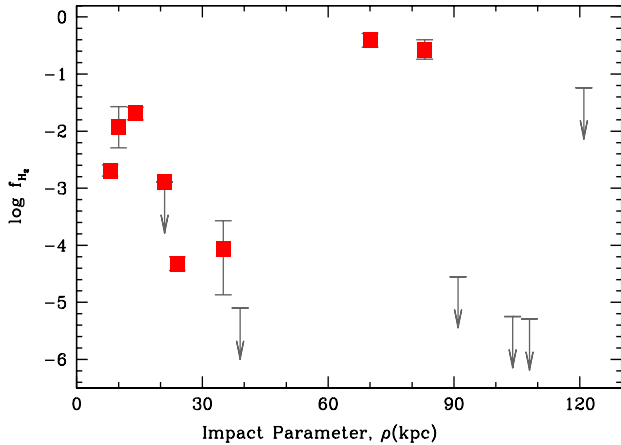


**Figure 9.** The molecular mass functions against the impact parameters of the nearest possible host-galaxies (see column 11 of Table 1). The arrows without squares represent systems where  $\text{H}_2$  is not detected.

the nearest possible host-galaxy candidate for these systems. There are five more systems where  $\text{H}_2$  absorption is not detected but the impact parameters of the nearest possible host-galaxy candidates are available. These are shown just by arrows in the figure. Note that all these five systems show  $\rho > 30$  kpc. In our limited sample, there is no obvious correlation between the  $f_{\text{H}_2}$  and the impact parameter. However, the  $\text{H}_2$  detection rate seems to be higher when the impact parameter is  $\rho < 30$  kpc.

We notice that three (five) of the eight systems show  $\rho < 20$  kpc (30 kpc). These are roughly consistent with the median values of impact parameters for the DLA/sub-DLA host-galaxies found by Rao et al. (2011). Nonetheless, the presence of the molecular gas at impact parameters of 15–40 kpc is surprising. We therefore put forward a scenario where molecular hydrogen detected in DLAs/sub-DLAs is not related to star-forming disks but stems from halo gas. However, the density range of halo gas as suggested by the low ionization metal lines (e.g. Muzahid 2014; Werk et al. 2014), is too low for *in situ*  $\text{H}_2$  production. We thus speculate that the molecular gas is tidally stripped or ejected disk-material that retained a molecular phase partially due to self-shielding and the lower ambient UV radiation as suggested from simple photoionization models. The detections of molecular hydrogen in high velocity clouds (Richter et al. 2001) and in the leading arm of the Magellanic Stream (Sembach et al. 2001) reinforce such an idea (see also Crighton et al. 2013).

Radio observations of the H I 21-cm line is another powerful tool for studying cold and neutral gas (Gupta et al. 2007, 2012) and diagnoses physical conditions in host-galaxies when detected (Gupta et al. 2013; Borthakur et al. 2014). The only system with  $\rho < 10$  kpc (i.e.  $z_{\text{abs}} = 0.10115$  towards Q 0439–433) shows a tentative detection of 21-cm absorption (Kanekar et al. 2001). Even in this case the QSO sight line is well beyond the stellar disk of the galaxy (Petitjean et al. 1996). A detailed analysis of this system with follow up VLBA observations will be presented by Dutta et al. (2014, in preparation).

It is apparent from Fig. 9 that the two systems showing the highest molecular fractions in our sample are detected at the largest impact parameters, i.e.  $\rho \sim 80$  kpc. As discussed above, while  $\text{H}_2$  producing cold gas is expected at low impact parameters (e.g.  $\rho \lesssim 10$  kpc), systems at  $\rho \sim 80$  kpc with a molecular fraction of

$\sim 1/10$  are extremely surprising. The impact parameters for these two systems come from Oliveira et al. (2014, towards B0120-28) and Werk et al. (2013, towards J0925+4004). In addition to  $\text{H}_2$ , a detection of the HD molecule has been reported in the former system. We do not have the image of this field accessible to us to make any comment on the host-galaxy. However, we note that the molecular hydrogen is detected in four different components spread over  $\sim 180 \text{ km s}^{-1}$ , implying a high volume filling factor of  $\text{H}_2$  clouds in this absorber. Naively, one would expect such a case when a line-of-sight is passing through the stellar (or H I) disk of a galaxy, requiring a much lower impact parameter. In fact, for the two other systems in our sample showing multiple  $\text{H}_2$  absorption components (i.e.  $z_{\text{abs}} = 0.10115$  towards Q 0439–433 and  $z_{\text{abs}} = 0.55733$  towards Q 0107–0232) show impact parameters of  $\sim 10$  kpc. Therefore, this system is of particular interest for future deep observations. The later system is a part of the ‘‘COS-Halos’’ sample (Tumlinson et al. 2011; Werk et al. 2013), that were observed to investigate the circum-galactic medium of isolated  $L_*$  galaxies at  $z \sim 0.2$ . Nonetheless, we note that Werk et al. (2012) have found two candidate galaxies in the QSO J 0925+4004 field at the redshift of the absorber with impact parameters of 81 and 92 kpc respectively. This possibly could mean that the  $\text{H}_2$  absorption is originating from a group environment and perhaps is not related to a halo of a single galaxy. We also note that two very faint photometric objects at  $\rho \lesssim 20$  kpc, at the absorber’s redshift, are seen in the SDSS image. Therefore, we can not rule out the possibility of one these objects being the true host-galaxy candidate. Deep images and determination of spectroscopic redshifts of all the photometric objects in this field are essential for understanding the true origin of molecular gas in this system.

## 6 SUMMARY

We have conducted a systematic search for molecular hydrogen ( $\text{H}_2$ ) in low redshift ( $z < 0.7$ ) DLAs and sub-DLAs using the medium resolution *HST*/COS spectra that were available in the public *HST* archive before March, 2014. This is the first-ever systematic search for  $\text{H}_2$  below the atmospheric cutoff. In total we found 33 DLAs/sub-DLAs with  $\log N(\text{H I}) \gtrsim 19$ , of which  $\text{H}_2$  information is available for 27 systems.  $\text{H}_2$  absorption from different rotational levels (up to  $J = 3$ ) is seen in a total of 10/27 systems, 3/5 in DLAs and 7/22 in sub-DLAs. Three  $\text{H}_2$  systems were reported previously by Crighton et al. (2013), Oliveira et al. (2014), and Srianand et al. (2014). The main findings of our analyses are summarized below:

- The incidence rate of  $\text{H}_2$  is generally higher at low- $z$  compared to that of the high- $z$  sample of N08, for different  $N(\text{H}_2)$  threshold values up to  $\log N(\text{H}_2) = 16.5$ . For systems with  $N(\text{H}_2) > 10^{14.4} \text{ cm}^{-2}$ , detected in spectra that are sensitive down to  $\log N(\text{H}_2) = 14.4$ , the incidence rate of  $\text{H}_2$  is  $50^{+25}_{-12}$  percent. This is a factor of  $\gtrsim 2$  higher than that of the high- $z$  sample. The difference in the incidence rate has a  $2\sigma$  level significance.
- There is no obvious threshold value of  $N(\text{H I})$  above which  $\text{H}_2$  is detected in our sample. A two-sided KS test suggests that there is no significant difference between the  $N(\text{H I})$  distributions for systems with and without molecular hydrogen. This is also true for the sample of N08. This implies that DLAs/sub-DLAs at any given redshift trace a wide range of physical conditions.
- The  $N(\text{H I})$  distribution of the high- $z$  sample of N08 is significantly different compared to our low- $z$  sample. The median  $\log N(\text{H I}) = 19.6$  as derived for our low- $z$  sample is 10 times

lower than that of the high- $z$  sample. Interestingly, the  $N(H_2)$  distribution, for systems where  $H_2$  is detected, do not show any significant difference between high- and low- $z$ .

- The  $f_{H_2}$  distribution for our low- $z$  sample is significantly different compared to those of the Galactic disk/halo and the Magellanic Clouds. Only a mild difference is noticed between the  $f_{H_2}$  distributions at low- and high- $z$  for the entire sample. However, no difference is suggested when we consider only systems with  $\log f_{H_2} > -4.9$ . The mild difference inferred for the entire sample is the manifestation of the fact that the  $H_2$  detection rate is considerably higher at low- $z$  than at high- $z$ .

- For the components where  $H_2$  is detected with a total  $N(H_2) > 10^{16.5} \text{ cm}^{-2}$ , the median rotational excitation temperature is found to be  $T_{01} = 133 \pm 55 \text{ K}$ . This is consistent with what has been seen in the “high- $z$  DLAs” (e.g.  $143 \pm 19 \text{ K}$ ). The inferred  $T_{01}$  are, however, slightly higher than those derived for the Galactic disk (i.e.  $77 \pm 17$  (rms) K, Savage et al. 1977), the Galactic halo (i.e.  $115 \pm 13 \text{ K}$ , Gillmon et al. 2006), and the Magellanic Clouds (i.e.  $82 \pm 21$  (rms) K, Tumlinson et al. 2002).

- Low- $z$   $H_2$  systems occupy a unique region in the  $f_{H_2} - N_{H\text{I}}$  plane (i.e.  $\log f_{H_2} \gtrsim -4.5$  and  $\log N(H_2) \lesssim 20.7$ ). Only a handful of  $H_2$  systems from the high- $z$  and the Galactic disk/Magellanic Cloud samples fall in this regime of parameter-space. Interestingly, a significant fraction (i.e. 25/40) of the Galactic halo systems, with detected  $H_2$ , show similar range in  $f_{H_2}$  and  $N_{H\text{I}}$ .

- Eight out of 10 systems, where  $H_2$  is detected, have host-galaxy information available from the literature. The majority of them (7/8) show impact parameters  $\rho > 10 \text{ kpc}$ , suggesting that they are perhaps not originating from the luminous disks of the host-galaxies. We notice that even for the system with the lowest impact parameter (i.e.  $\rho = 8 \text{ kpc}$  for the  $z_{\text{abs}} = 0.10115$  towards Q 0439–433 system) the line of sight is outside the luminous stellar disk. The two systems with the highest molecular fractions (e.g.  $\log f_{H_2} > -1.0$ ) show the largest impact parameters (i.e.  $\rho \sim 80 \text{ kpc}$ ). Searching for sub- $L_*$  galaxies close to these QSO lines of sight is indispensable for understanding the possible origin(s) of  $H_2$  absorption in low- $z$  DLAs/sub-DLAs.

- Using simple photoionization models we have shown that if the low- $z$   $H_2$  systems have density in the range  $10 - 100 \text{ cm}^{-3}$ , as for high- $z$   $H_2$  systems (Srianand et al. 2005), the radiation field prevailing in these absorbers cannot have an appreciable stellar contribution. This is also consistent with the origin of these low- $z$   $H_2$  systems in locations far from galactic disks. Detailed ionization models for these systems, with further observational constraints from additional low, intermediate, and high ionization metal lines, will be presented in forthcoming papers.

SM thankfully acknowledge Dr. Eric Feigelson for useful discussions on various statistical tests, survival analysis in particular.

## REFERENCES

Albornoz Vásquez, D., Rahmani, H., Noterdaeme, P., Petitjean, P., Srianand, R., & Ledoux, C., 2014, *A&A*, 562, A88  
 Bailly, D., Salumbides, E. J., Vervloet, M., & Ubachs, W., 2010, *Molecular Physics*, 108, 827  
 Balashev, S. A., Klimenko, V. V., Ivanchik, A. V., Varshalovich, D. A., Petitjean, P., & Noterdaeme, P., 2014, *MNRAS*, 440, 225  
 Battisti, A. J., Meiring, J. D., Tripp, T. M., et al., 2012, *ApJ*, 744, 93  
 Bekki, K., 2014, *MNRAS*, 444, 1615

Borthakur, S., Momjian, E., Heckman, T. M., York, D. G., Bowen, D. V., Yun, M. S., & Tripp, T. M., 2014, *ArXiv e-prints*  
 Bouwens, R. J., Illingworth, G. D., Oesch, P. A., et al., 2011, *ApJ*, 737, 90  
 Christensen, L., Wisotzki, L., Roth, M. M., Sánchez, S. F., Kelz, A., & Jahnke, K., 2007, *A&A*, 468, 587  
 Crighton, N. H. M., Bechtold, J., Carswell, R. F., et al., 2013, *MNRAS*, 433, 178  
 Danforth, C. W., Stocke, J. T., & Shull, J. M., 2010, *ApJ*, 710, 613  
 Ferland, G. J., Porter, R. L., van Hoof, P. A. M., et al., 2013, *Rev. Mexicana Astron. Astrofis.*, 49, 137  
 Fynbo, J. P. U., Laursen, P., Ledoux, C., et al., 2010, *MNRAS*, 408, 2128  
 Gehrels, N., 1986, *ApJ*, 303, 336  
 Ghavamian, P., Aloisi, A., Lennon, D., et al., 2009, *Preliminary Characterization of the Post-Launch Line Spread Function of COS*. Tech. rep.  
 Gillmon, K., Shull, J. M., Tumlinson, J., & Danforth, C., 2006, *ApJ*, 636, 891  
 Gould, R. J. & Salpeter, E. E., 1963, *ApJ*, 138, 393  
 Green, J. C., Froning, C. S., Osterman, S., et al., 2012, *ApJ*, 744, 60  
 Guimarães, R., Noterdaeme, P., Petitjean, P., Ledoux, C., Srianand, R., López, S., & Rahmani, H., 2012, *AJ*, 143, 147  
 Gupta, N., Srianand, R., Noterdaeme, P., Petitjean, P., & Muzahid, S., 2013, *A&A*, 558, A84  
 Gupta, N., Srianand, R., Petitjean, P., Bergeron, J., Noterdaeme, P., & Muzahid, S., 2012, *A&A*, 544, A21  
 Gupta, N., Srianand, R., Petitjean, P., Khare, P., Saikia, D. J., & York, D. G., 2007, *ApJ*, 654, L111  
 Haardt, F. & Madau, P., 1996, *ApJ*, 461, 20  
 —, 2001, in *Clusters of Galaxies and the High Redshift Universe Observed in X-rays*, Neumann, D. M. & Tran, J. T. V., eds.  
 —, 2012, *ApJ*, 746, 125  
 Habing, H. J., 1968, *Bull. Astron. Inst. Netherlands*, 19, 421  
 Hellsten, U., Hernquist, L., Katz, N., & Weinberg, D. H., 1998, *ApJ*, 499, 172  
 Hollenbach, D. & Salpeter, E. E., 1971, *ApJ*, 163, 155  
 Jenkins, E. B. & Peimbert, A., 1997, *ApJ*, 477, 265  
 Jorgenson, R. A., Murphy, M. T., Thompson, R., & Carswell, R. F., 2014, *MNRAS*, 443, 2783  
 Jorgenson, R. A. & Wolfe, A. M., 2014, *ApJ*, 785, 16  
 Kacprzak, G. G., Churchill, C. W., Evans, J. L., Murphy, M. T., & Steidel, C. C., 2011, *MNRAS*, 416, 3118  
 Kanekar, N., Chengalur, J. N., Subrahmanyam, R., & Petitjean, P., 2001, *A&A*, 367, 46  
 Kriss, G. A., 2011, *Improved Medium Resolution Line Spread Functions for COS FUV Spectra*. Tech. rep.  
 Kulkarni, V. P., Fall, S. M., Lauroesch, J. T., York, D. G., Welty, D. E., Khare, P., & Truran, J. W., 2005, *ApJ*, 618, 68  
 Kulkarni, V. P., Khare, P., Péroux, C., York, D. G., Lauroesch, J. T., & Meiring, J. D., 2007, *ApJ*, 661, 88  
 Kulkarni, V. P., Woodgate, B. E., York, D. G., Thatte, D. G., Meiring, J., Palunas, P., & Wassell, E., 2006, *ApJ*, 636, 30  
 Lanzetta, K. M., Wolfe, A. M., Altan, H., et al., 1997, *AJ*, 114, 1337  
 Ledoux, C., Petitjean, P., Fynbo, J. P. U., Møller, P., & Srianand, R., 2006a, *A&A*, 457, 71  
 Ledoux, C., Petitjean, P., & Srianand, R., 2003, *MNRAS*, 346, 209  
 —, 2006b, *ApJ*, 640, L25  
 Meiring, J. D., Tripp, T. M., Prochaska, J. X., et al., 2011, *ApJ*,

- 732, 35
- Meiring, J. D., Tripp, T. M., Werk, J. K., Howk, J. C., Jenkins, E. B., Prochaska, J. X., Lehner, N., & Sembach, K. R., 2013, *ApJ*, 767, 49
- Møller, P., Fynbo, J. P. U., & Fall, S. M., 2004, *A&A*, 422, L33
- Muzahid, S., 2014, *ApJ*, 784, 5
- Noterdaeme, P., Laursen, P., Petitjean, P., et al., 2012a, *A&A*, 540, A63
- Noterdaeme, P., Ledoux, C., Petitjean, P., & Srianand, R., 2008a, *A&A*, 481, 327
- Noterdaeme, P., Ledoux, C., Srianand, R., Petitjean, P., & Lopez, S., 2009a, *A&A*, 503, 765
- Noterdaeme, P., Petitjean, P., Carithers, W. C., et al., 2012b, *A&A*, 547, L1
- Noterdaeme, P., Petitjean, P., Ledoux, C., López, S., Srianand, R., & Vergani, S. D., 2010, *A&A*, 523, A80
- Noterdaeme, P., Petitjean, P., Ledoux, C., & Srianand, R., 2009b, *A&A*, 505, 1087
- Noterdaeme, P., Petitjean, P., Ledoux, C., Srianand, R., & Ivanchik, A., 2008b, *A&A*, 491, 397
- Noterdaeme, P., Petitjean, P., Srianand, R., Ledoux, C., & Le Petit, F., 2007, *A&A*, 469, 425
- Obreschkow, D. & Rawlings, S., 2009, *ApJ*, 696, L129
- Oliveira, C. M., Sembach, K. R., Tumlinson, J., O'Meara, J., & Thom, C., 2014, *ApJ*, 783, 22
- Osterman, S., Green, J., Froning, C., et al., 2011, *Ap&SS*, 335, 257
- Péroux, C., Bouché, N., Kulkarni, V. P., York, D. G., & Vladilo, G., 2011, *MNRAS*, 410, 2237
- Péroux, C., Dessauges-Zavadsky, M., D'Odorico, S., Kim, T.-S., & McMahon, R. G., 2003a, *MNRAS*, 345, 480
- Péroux, C., McMahon, R. G., Storrie-Lombardi, L. J., & Irwin, M. J., 2003b, *MNRAS*, 346, 1103
- Petitjean, P., Ledoux, C., Noterdaeme, P., & Srianand, R., 2006, *A&A*, 456, L9
- Petitjean, P., Srianand, R., & Ledoux, C., 2002, *MNRAS*, 332, 383
- Petitjean, P., Theodore, B., Smette, A., & Lespine, Y., 1996, *A&A*, 313, L25
- Pettini, M., Smith, L. J., King, D. L., & Hunstead, R. W., 1997, *ApJ*, 486, 665
- Prochaska, J. X., Gawiser, E., Wolfe, A. M., Castro, S., & Djorgovski, S. G., 2003, *ApJ*, 595, L9
- Prochaska, J. X. & Wolfe, A. M., 2009, *ApJ*, 696, 1543
- Rafelski, M., Wolfe, A. M., Prochaska, J. X., Neeleman, M., & Mendez, A. J., 2012, *ApJ*, 755, 89
- Rao, S. M., Belfort-Mihalyi, M., Turnshek, D. A., Monier, E. M., Nestor, D. B., & Quider, A., 2011, *MNRAS*, 416, 1215
- Rao, S. M. & Turnshek, D. A., 2000, *ApJS*, 130, 1
- Rao, S. M., Turnshek, D. A., & Nestor, D. B., 2006, *ApJ*, 636, 610
- Richter, P., Sembach, K. R., Wakker, B. P., & Savage, B. D., 2001, *ApJ*, 562, L181
- Rodríguez, E., Petitjean, P., Aracil, B., Ledoux, C., & Srianand, R., 2006, *A&A*, 446, 791
- Roy, N., Chengalur, J. N., & Srianand, R., 2006, *MNRAS*, 365, L1
- Savage, B. D., Bohlin, R. C., Drake, J. F., & Budich, W., 1977, *ApJ*, 216, 291
- Savage, B. D., Narayanan, A., Lehner, N., & Wakker, B. P., 2011, *ApJ*, 731, 14
- Schaye, J., Aguirre, A., Kim, T.-S., Theuns, T., Rauch, M., & Sargent, W. L. W., 2003, *ApJ*, 596, 768
- Sembach, K. R., Howk, J. C., Savage, B. D., & Shull, J. M., 2001, *AJ*, 121, 992
- Snow, T. P., Rachford, B. L., Tumlinson, J., et al., 2000, *ApJ*, 538, L65
- Som, D., Kulkarni, V. P., Meiring, J., York, D. G., Péroux, C., Khare, P., & Lauroesch, J. T., 2013, *MNRAS*, 435, 1469
- Springel, V., White, S. D. M., Jenkins, A., et al., 2005, *Nature*, 435, 629
- Srianand, R., Noterdaeme, P., Ledoux, C., & Petitjean, P., 2008, *A&A*, 482, L39
- Srianand, R., Petitjean, P., Ledoux, C., Ferland, G., & Shaw, G., 2005, *MNRAS*, 362, 549
- Srianand, R., Rahmani, H., Muzahid, S., & Mohan, V., 2014, *ArXiv e-prints*
- Tacconi, L. J., Neri, R., Chapman, S. C., et al., 2006, *ApJ*, 640, 228
- Tejos, N., Morris, S. L., Finn, C. W., et al., 2014, *MNRAS*, 437, 2017
- Tremonti, C. A., Heckman, T. M., Kauffmann, G., et al., 2004, *ApJ*, 613, 898
- Tripp, T. M., Jenkins, E. B., Bowen, D. V., Prochaska, J. X., Aracil, B., & Ganguly, R., 2005, *ApJ*, 619, 714
- Tumlinson, J., Malec, A. L., Carswell, R. F., et al., 2010, *ApJ*, 718, L156
- Tumlinson, J., Shull, J. M., Rachford, B. L., et al., 2002, *ApJ*, 566, 857
- Tumlinson, J., Werk, J. K., Thom, C., et al., 2011, *ApJ*, 733, 111
- Welty, D. E., Xue, R., & Wong, T., 2012, *ApJ*, 745, 173
- Werk, J. K., Prochaska, J. X., Thom, C., Tumlinson, J., Tripp, T. M., O'Meara, J. M., & Meiring, J. D., 2012, *ApJS*, 198, 3
- Werk, J. K., Prochaska, J. X., Thom, C., Tumlinson, J., Tripp, T. M., O'Meara, J. M., & Peebles, M. S., 2013, *ApJS*, 204, 17
- Werk, J. K., Prochaska, J. X., Tumlinson, J., et al., 2014, *ArXiv e-prints*
- Wolfe, A. M., Gawiser, E., & Prochaska, J. X., 2005, *ARA&A*, 43, 861
- Young, L. M., 2002, *AJ*, 124, 788
- Yozin, C. & Bekki, K., 2014, *MNRAS*, 443, 522
- Zwaan, M. A. & Prochaska, J. X., 2006, *ApJ*, 643, 675
- Zwaan, M. A., van der Hulst, J. M., Briggs, F. H., Verheijen, M. A. W., & Ryan-Weber, E. V., 2005, *MNRAS*, 364, 1467

APPENDIX A: VOIGT PROFILE FIT TO H I ABSORPTION LINES FOR SYSTEMS LISTED IN TABLE 1

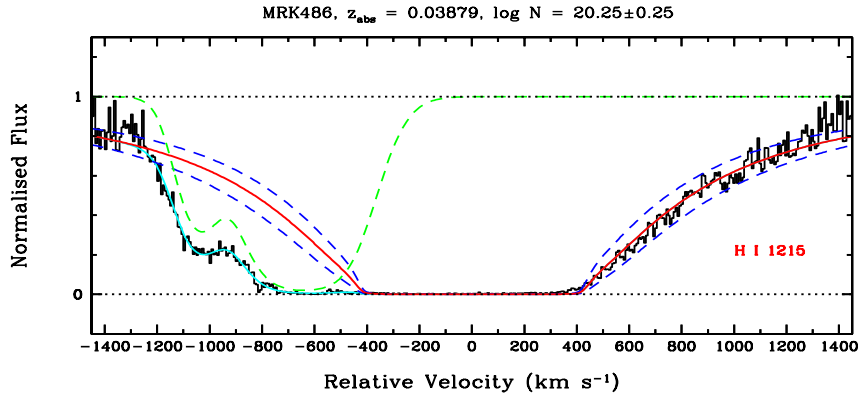


**Figure A1.** Damped Ly $\alpha$  absorption from  $z_{\text{abs}} = 0.03879$  towards MRK486 system. The red smooth and blue dashed curves plotted on the data (black histogram) are the best fitting Voigt profiles for the sub-DLA component and its  $1\sigma$  uncertainty. Unrelated absorption is usually fitted assuming Ly $\alpha$ . The green dashed curve at  $\sim 800 \text{ km s}^{-1}$  shows an unrelated absorption. Cyan curve represents the total (sub-DLA + unrelated) absorption model.

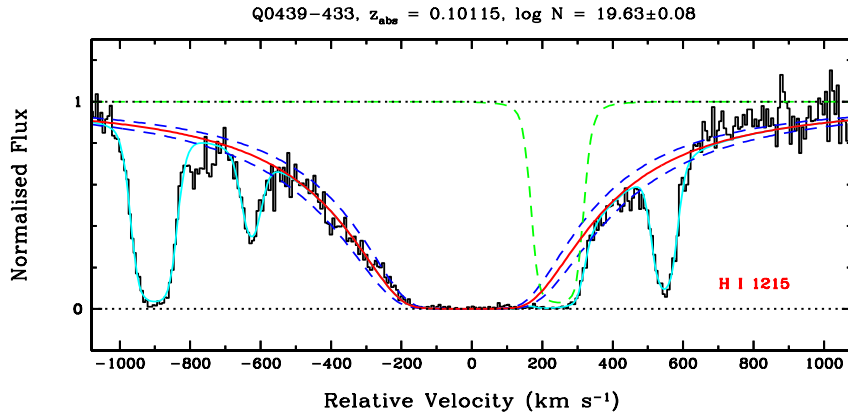


**Figure A2.** Sub-damped Ly $\alpha$  absorption from  $z_{\text{abs}} = 0.10115$  towards Q 0439-433 system. Various curves are as described in Fig. A1.

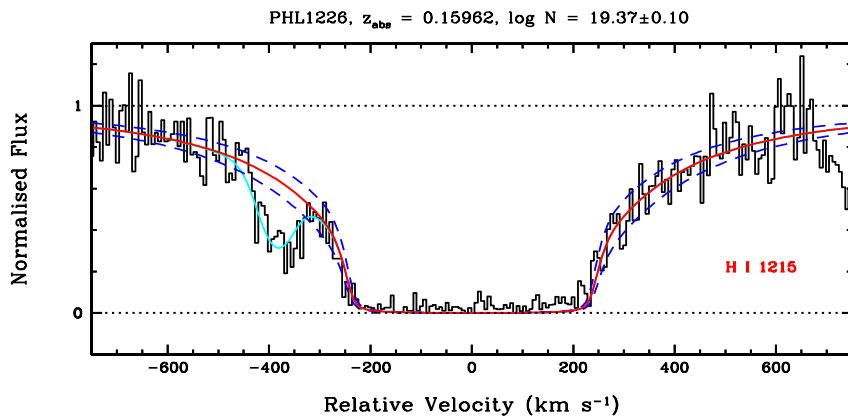


**Figure A3.** Sub-damped Ly $\alpha$  absorption from  $z_{\text{abs}} = 0.15962$  towards PHL1226 system. Various curves are as described in Fig. A1.

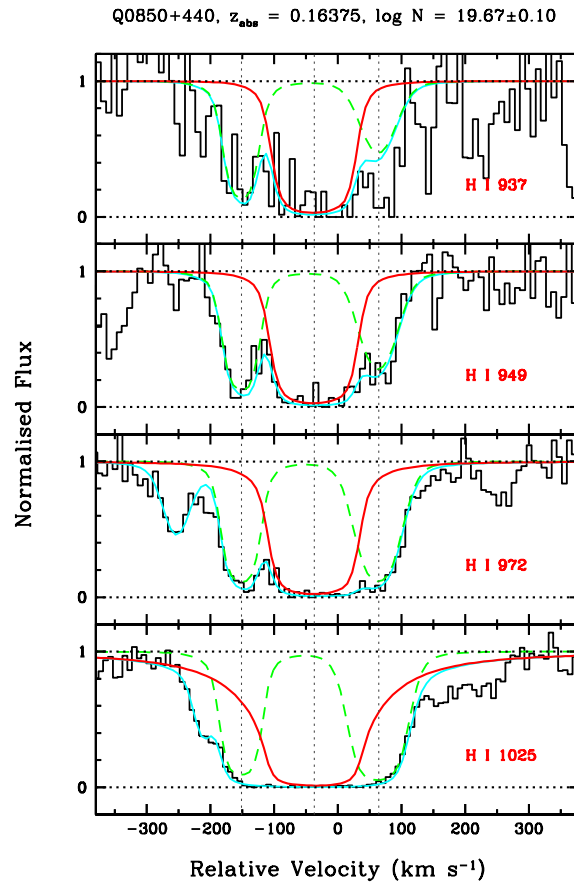


**Figure A4.** Lyman series absorption from  $z_{\text{abs}} = 0.16375$  towards Q 0850+440 system. Various curves are as described in Fig. A1.

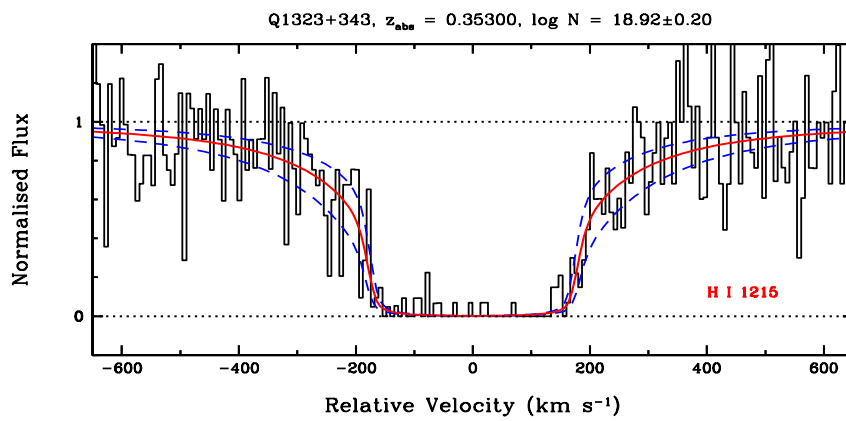


**Figure A5.** Sub-damped Ly $\alpha$  absorption from  $z_{\text{abs}} = 0.35300$  towards Q1323+343 system. Various curves are as described in Fig. A1.



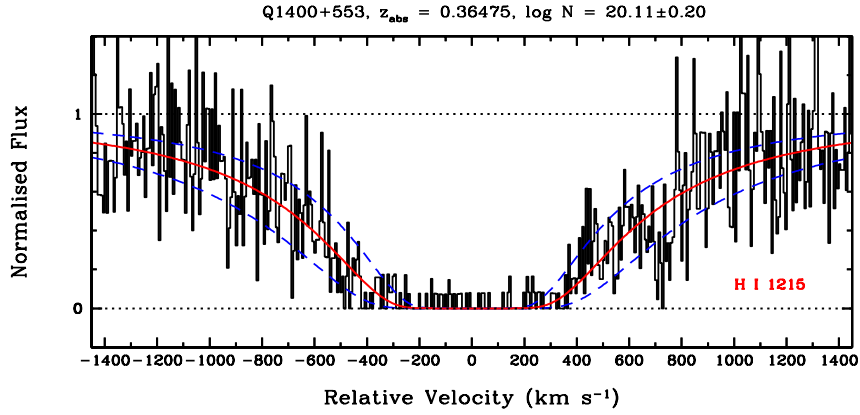


Figure A6. Damped Ly $\alpha$  absorption from  $z_{\text{abs}} = 0.36475$  towards Q1400+553 system. Various curves are as described in Fig. A1.

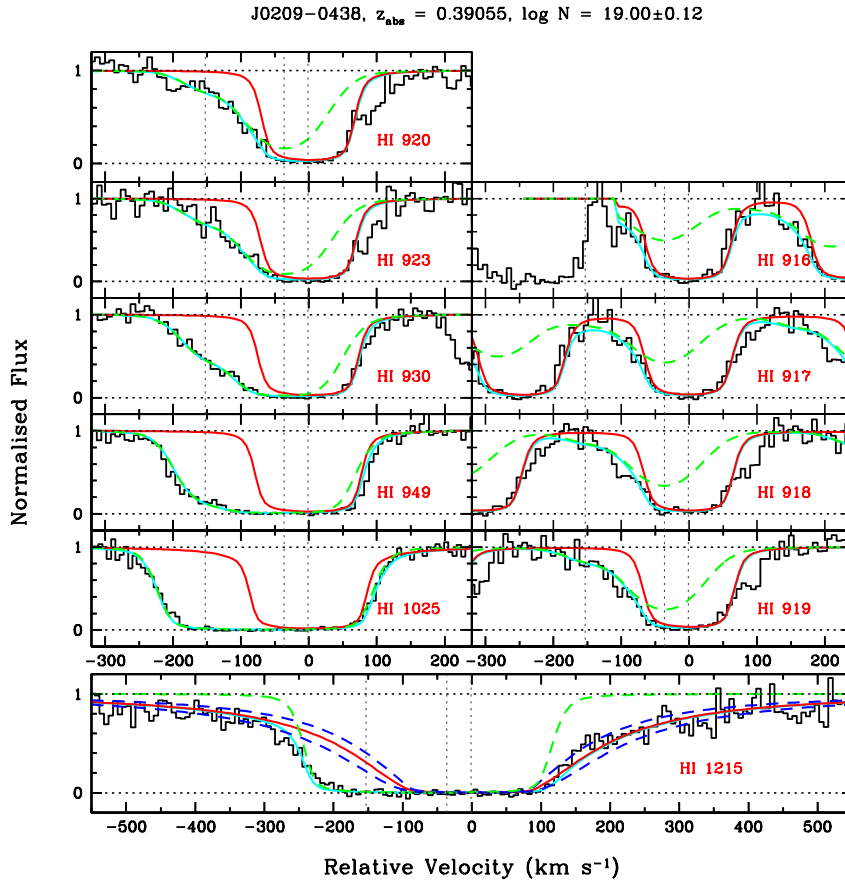
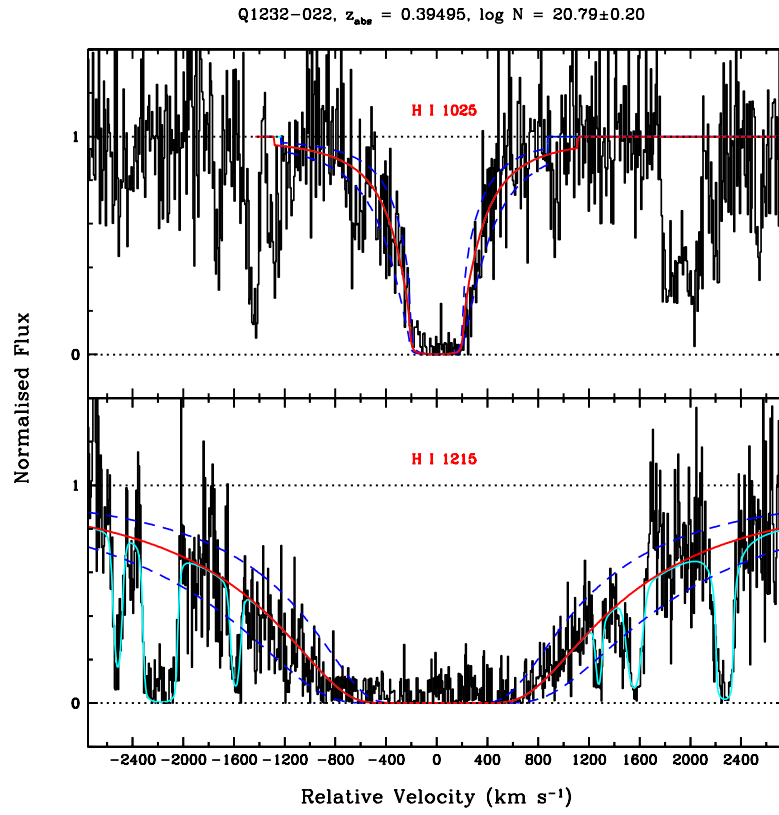
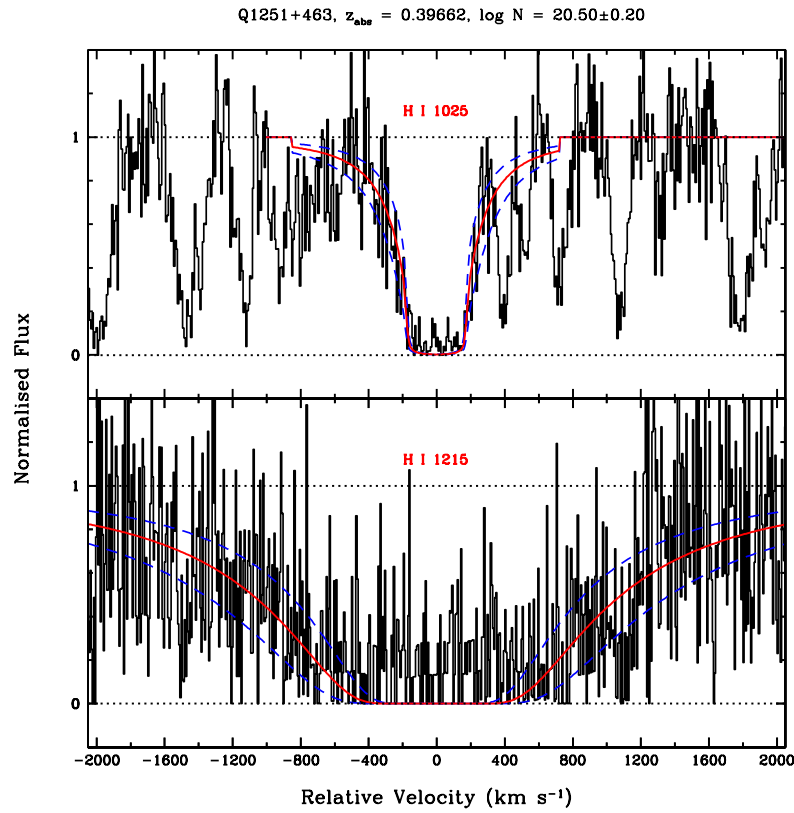


Figure A7. Lyman series absorption from  $z_{\text{abs}} = 0.39055$  towards J0209-0438 system. Various curves are as described in Fig. A1.



**Figure A8.** Damped Ly $\alpha$  and Ly $\beta$  absorption from  $z_{\text{abs}} = 0.39495$  towards Q1232-022 system. Various curves are as described in Fig. A1.



**Figure A9.** Damped Ly $\alpha$  and Ly $\beta$  absorption from  $z_{\text{abs}} = 0.39662$  towards Q1251+463 system. Various curves are as described in Fig. A1.

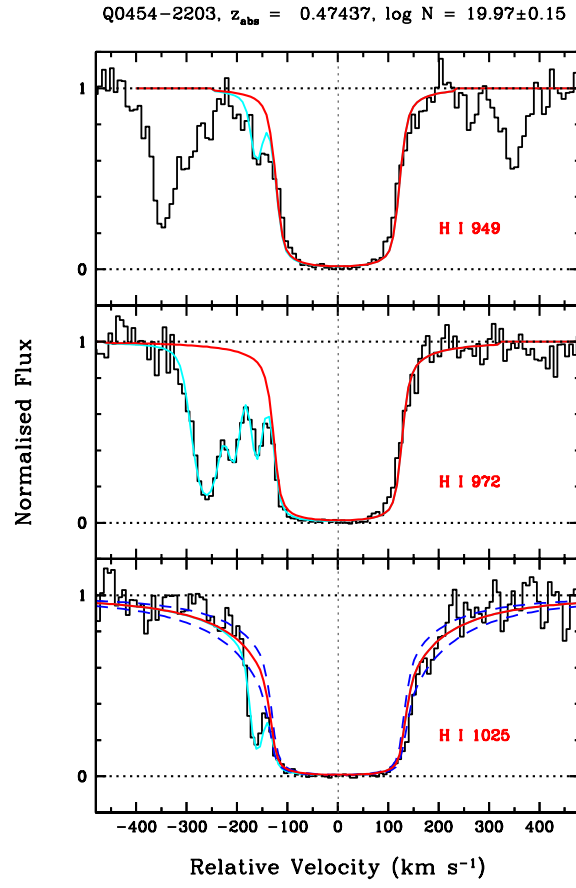


**Figure A10.** Lyman series absorption from  $z_{\text{abs}} = 0.47437$  towards Q0454-2203 system. Various curves are as described in Fig. A1.

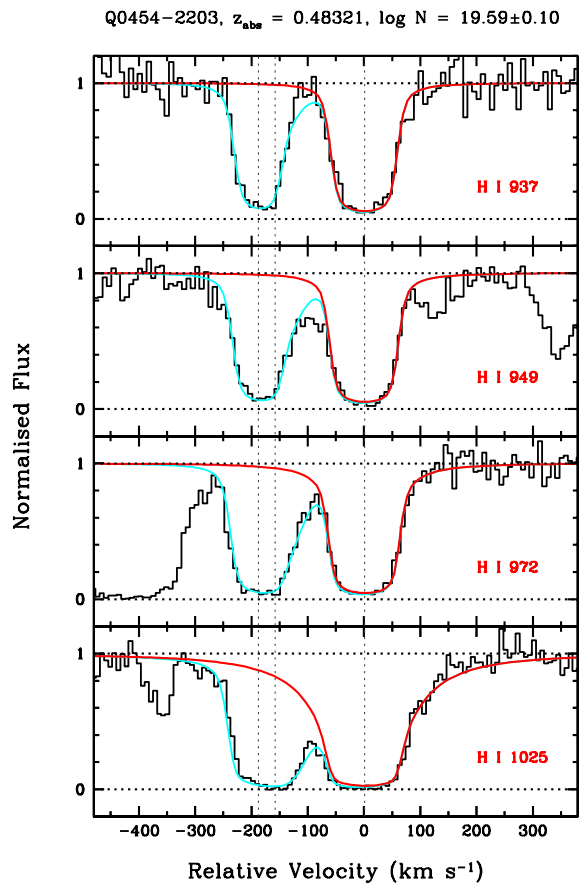


**Figure A11.** Lyman series absorption from  $z_{\text{abs}} = 0.48321$  towards Q0454-2203 system. Various curves are as described in Fig. A1.

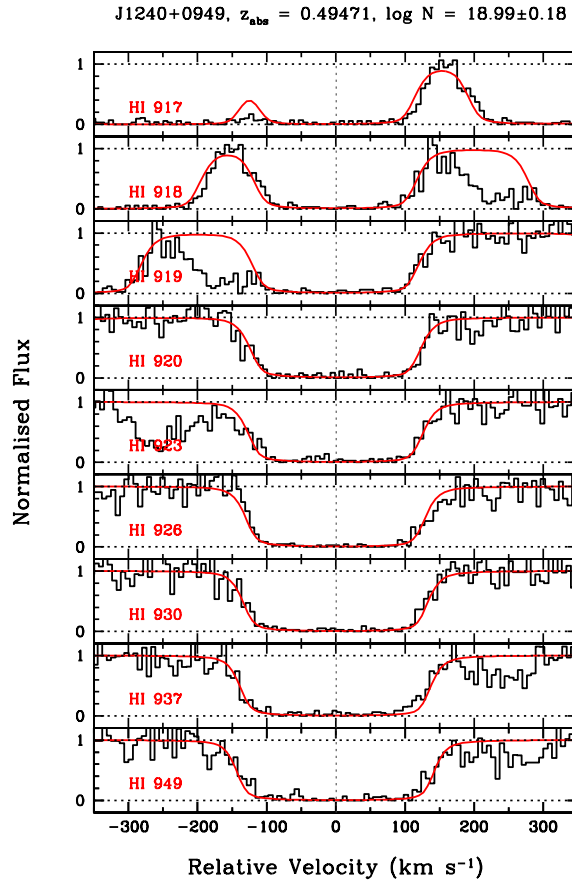


**Figure A12.** Lyman series absorption from  $z_{\text{abs}} = 0.49471$  towards J1240+0949 system. Various curves are as described in Fig. A1.

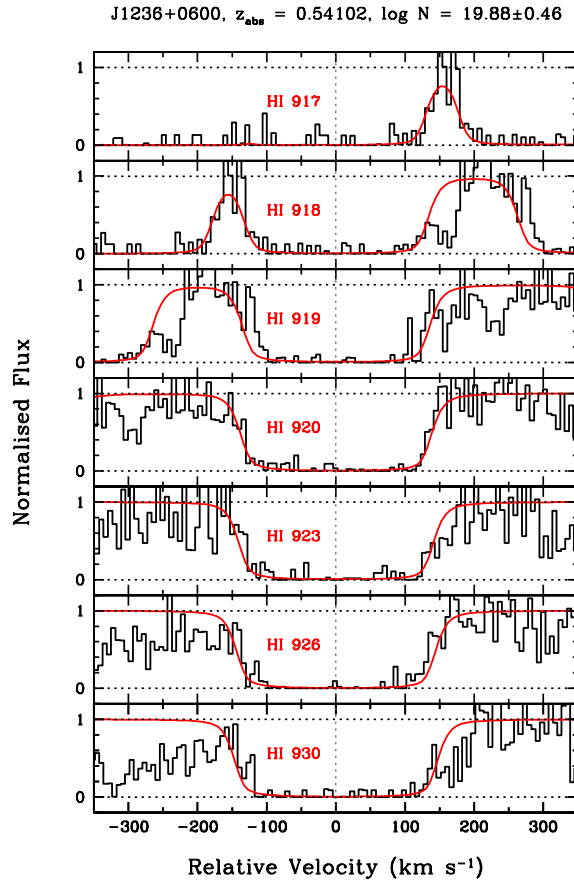


**Figure A13.** Lyman series absorption from  $z_{\text{abs}} = 0.54102$  towards J1236+0600 system. Various curves are as described in Fig. A1.

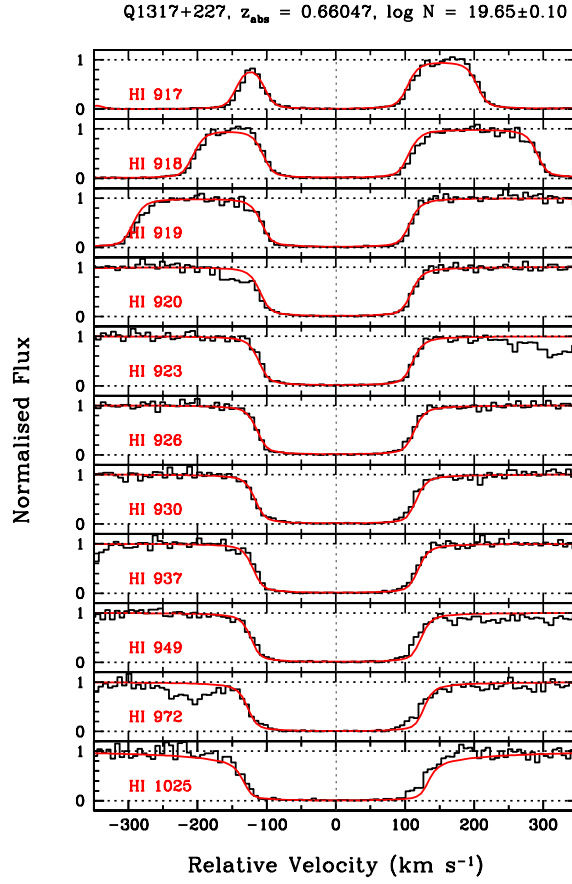


**Figure A14.** Lyman series absorption from  $z_{\text{abs}} = 0.66047$  towards Q1317+227 system. Various curves are as described in Fig. A1.

**APPENDIX B: VOIGT PROFILE FIT TO  $H I$  ABSORPTION LINES FOR SYSTEMS LISTED IN TABLE 2**

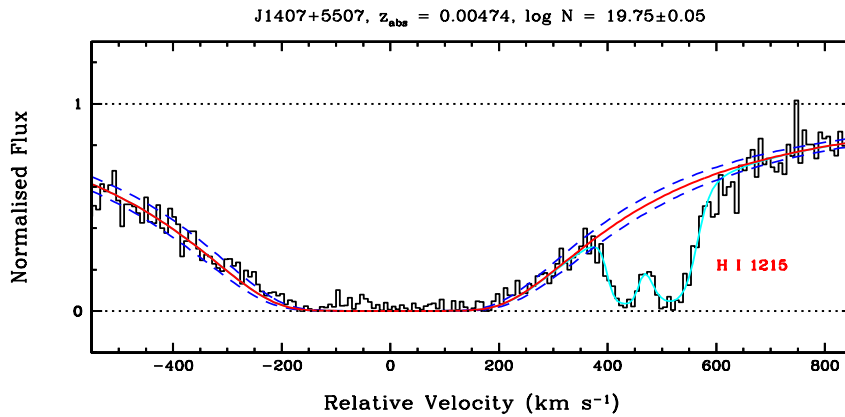


**Figure B1.** Sub-damped Ly $\alpha$  absorption from  $z_{\text{abs}} = 0.00474$  towards J1407+5507 system. The blue wing is affected by the Galactic Ly $\alpha$  absorption. Various curves are as described in Fig. A1.

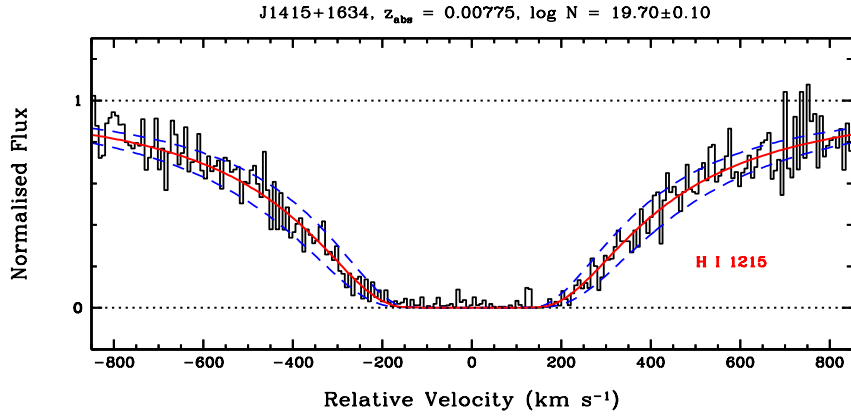


**Figure B2.** Sub-damped Ly $\alpha$  absorption from  $z_{\text{abs}} = 0.00775$  towards J1415+1634 system. Various curves are as described in Fig. A1.

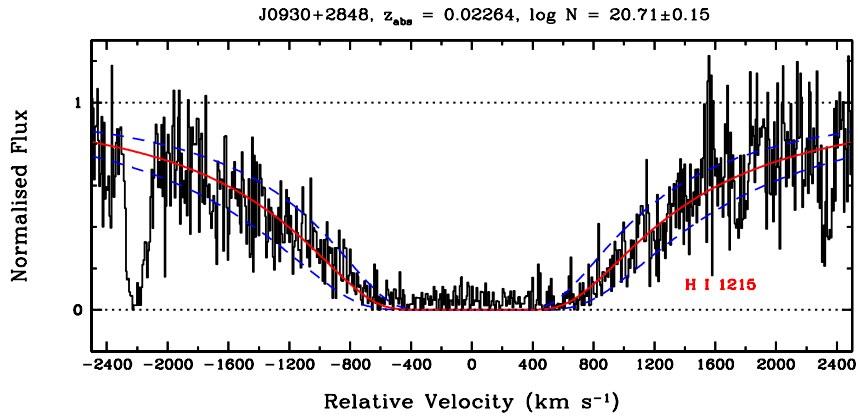


**Figure B3.** Damped Ly $\alpha$  absorption from  $z_{\text{abs}} = 0.02264$  towards J0930+2848 system. Various curves are as described in Fig. A1.

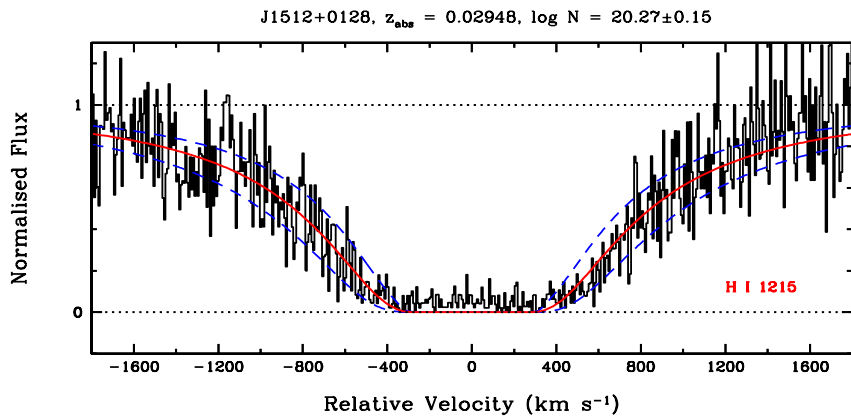


**Figure B4.** Damped Ly $\alpha$  absorption from  $z_{\text{abs}} = 0.02948$  towards J1512+0128 system. Various curves are as described in Fig. A1.



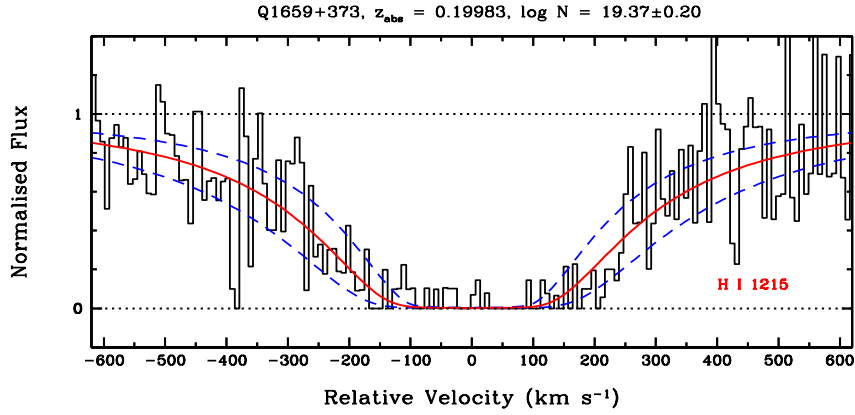


Figure B5. Sub-damped Ly $\alpha$  absorption from  $z_{\text{abs}} = 0.19983$  towards Q1659+373 system. Various curves are as described in Fig. A1.

APPENDIX C: VOIGT PROFILE FIT TO MOLECULAR HYDROGEN ABSORPTION

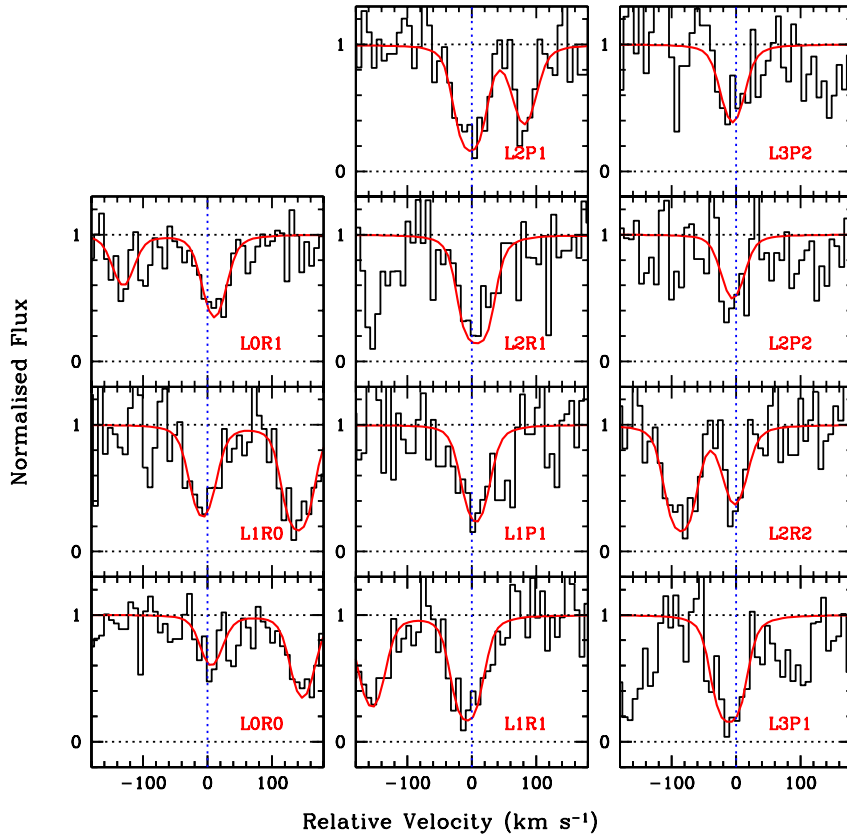
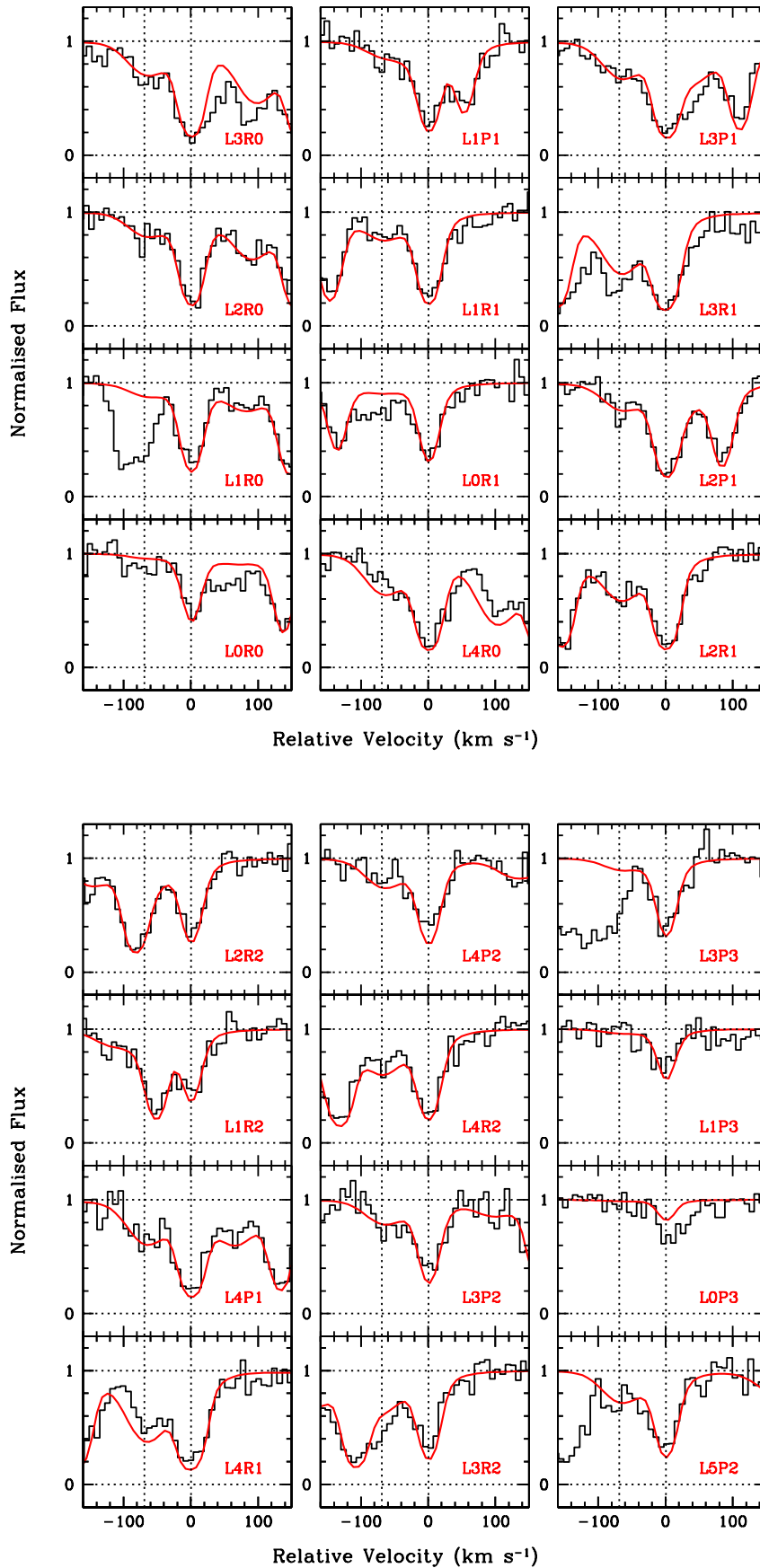


Figure C1. Molecular hydrogen absorption from the  $z_{\text{abs}} = 0.06650$  towards J1241+2852 system. The red smooth curves are the best fitting Voigt profiles to the data plotted in black histogram. The vertical dotted line marks the median line centroid.



**Figure C2.** Molecular hydrogen absorption from the  $z_{\text{abs}} = 0.10115$  towards Q0439–433 system. A weak component is possibly detected at  $\sim 70$  km s<sup>-1</sup>.

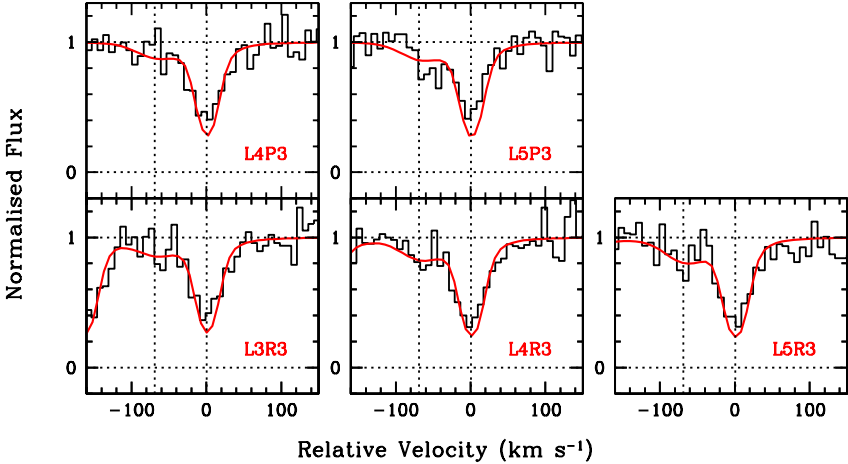


Figure C2. Continued.

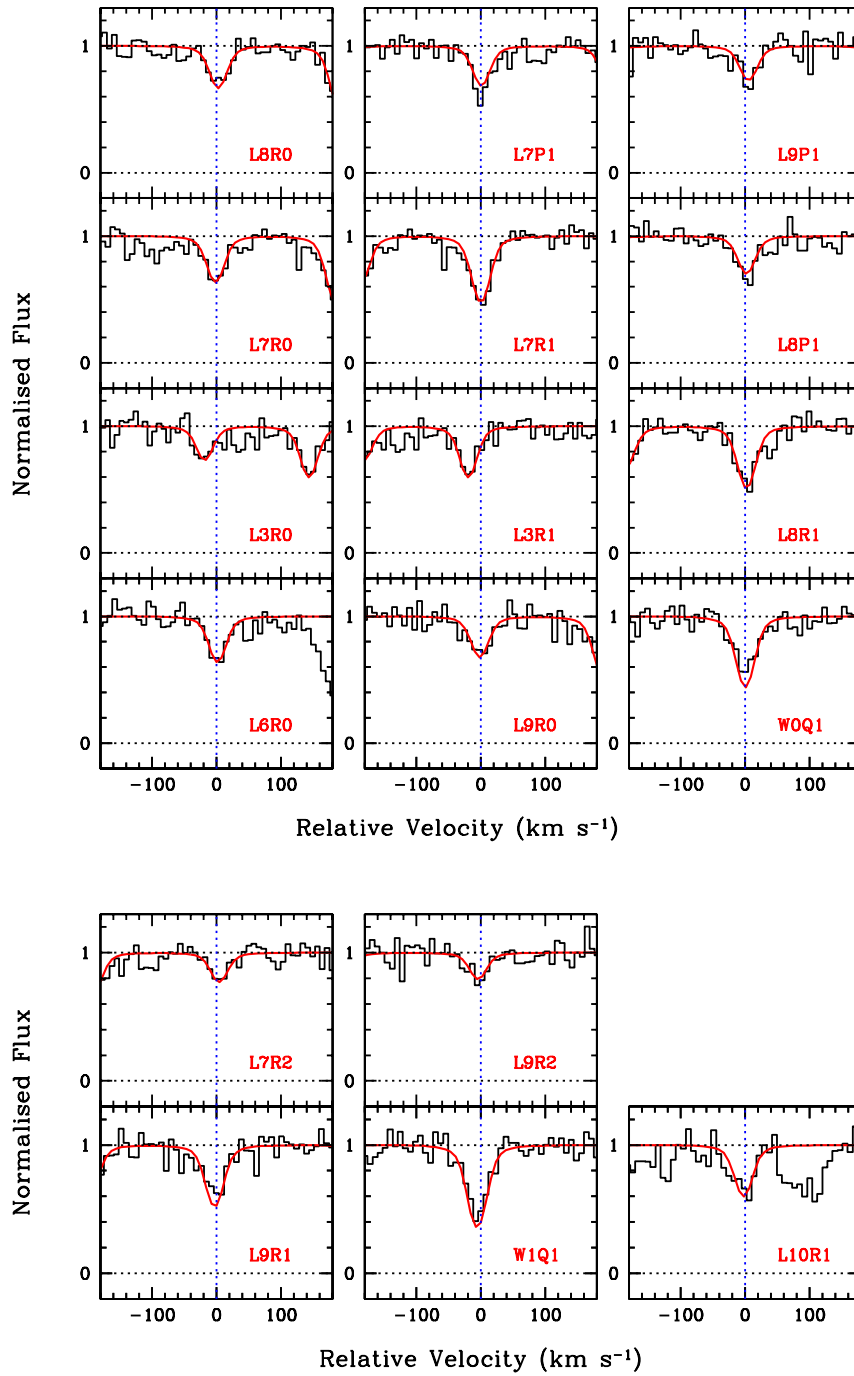


Figure C3. Molecular hydrogen absorption from the  $z_{\text{abs}} = 0.16375$  towards Q0850+440 system.

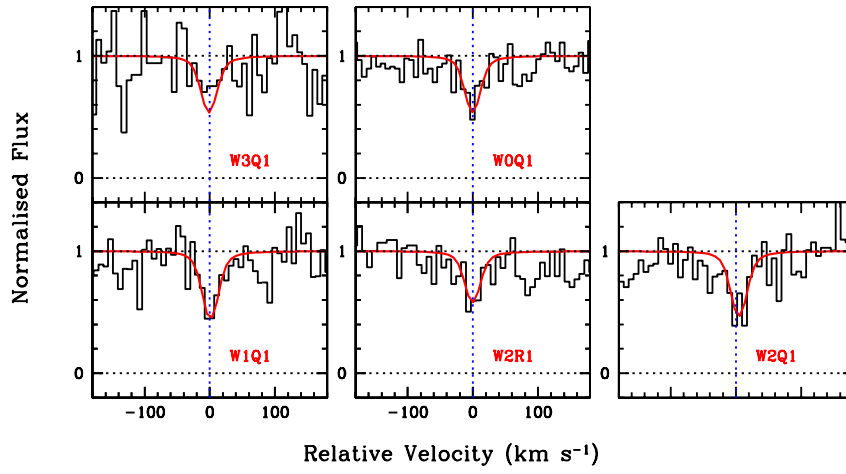


Figure C4. Molecular hydrogen absorption from the  $z_{\text{abs}} = 0.22711$  towards J1342-0053 system.

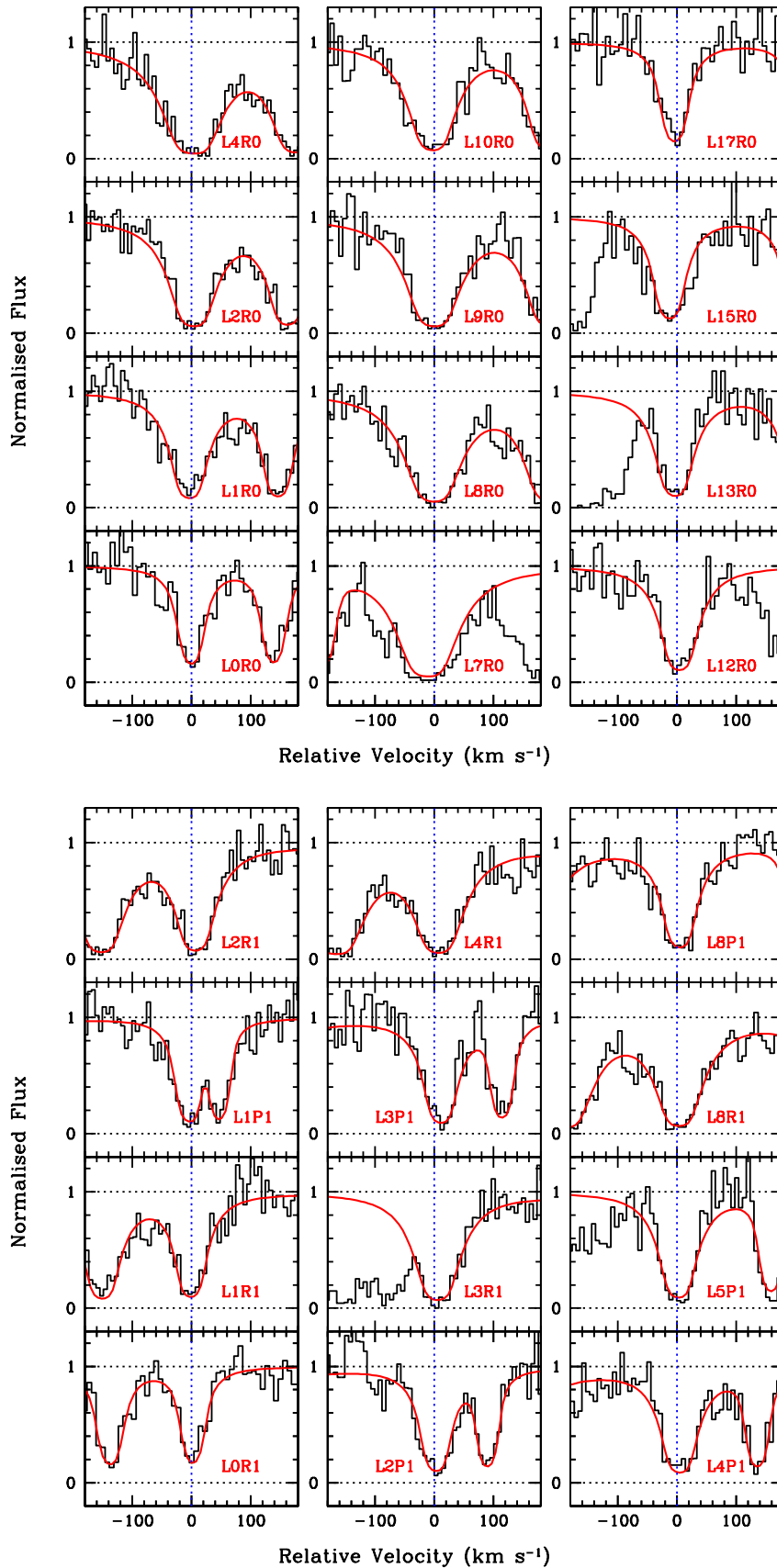


Figure C5. Molecular hydrogen absorption from the  $z_{\text{abs}} = 0.32110$  towards J1616+4154 system.

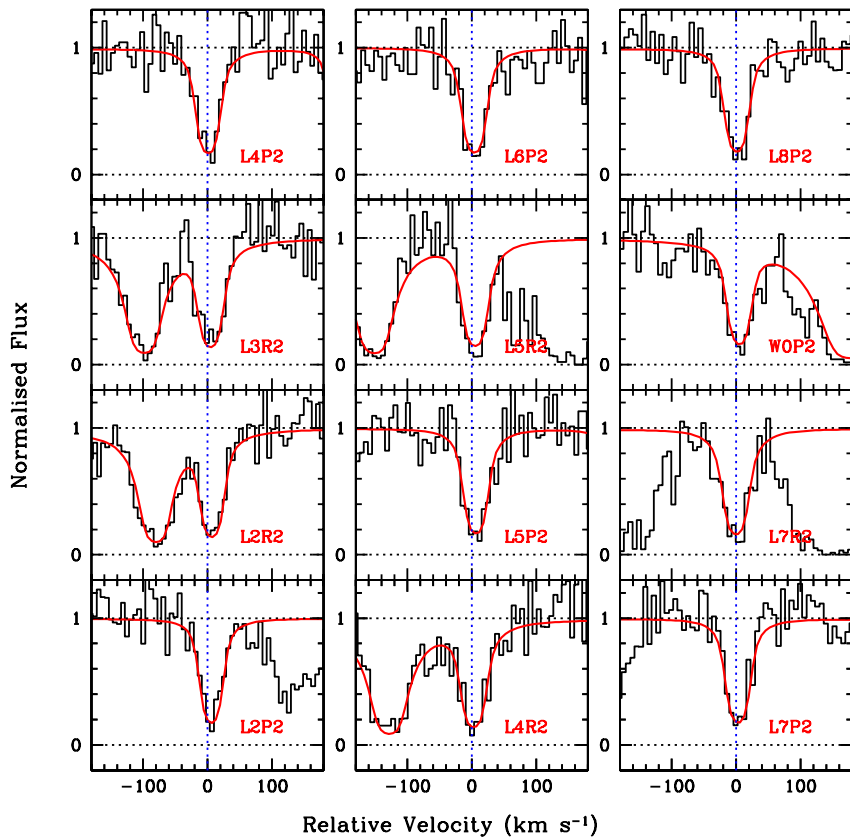
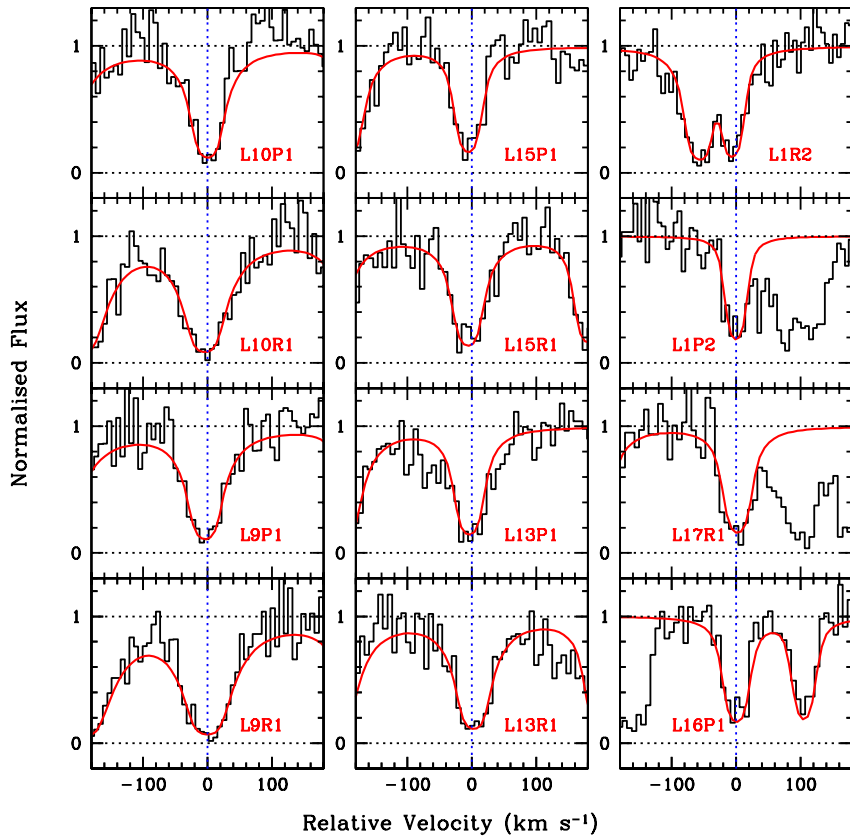


Figure C5. Continued.

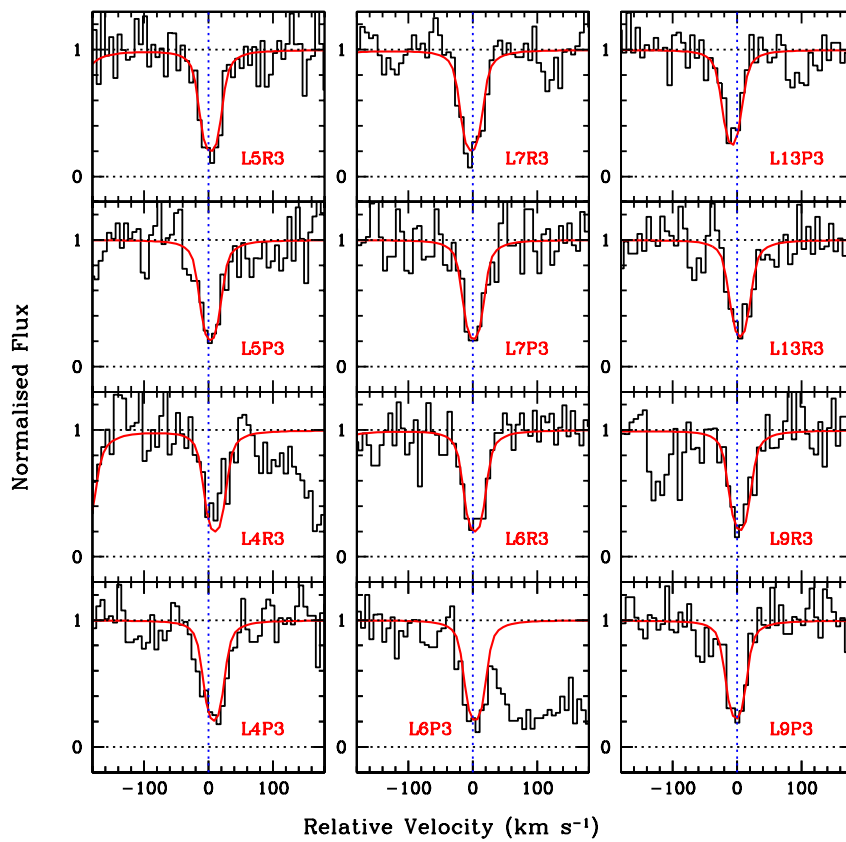
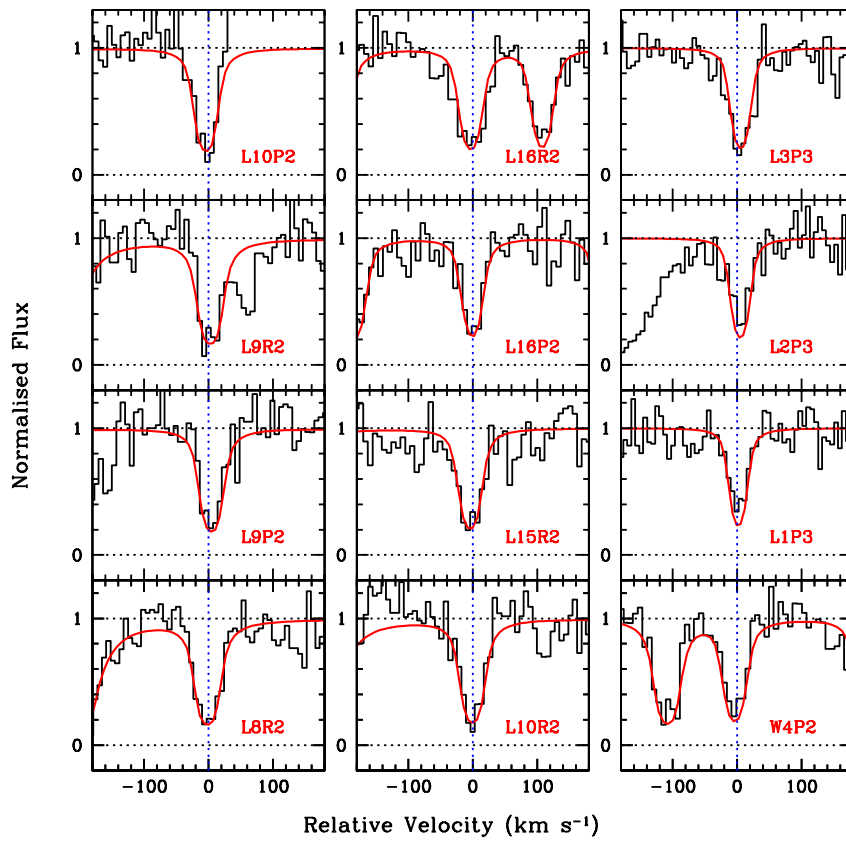


Figure C5. Continued.



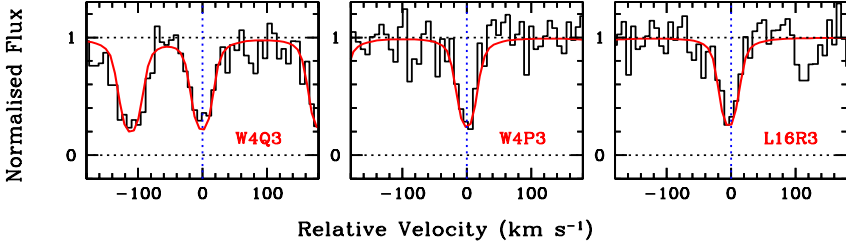


Figure C5. Continued.

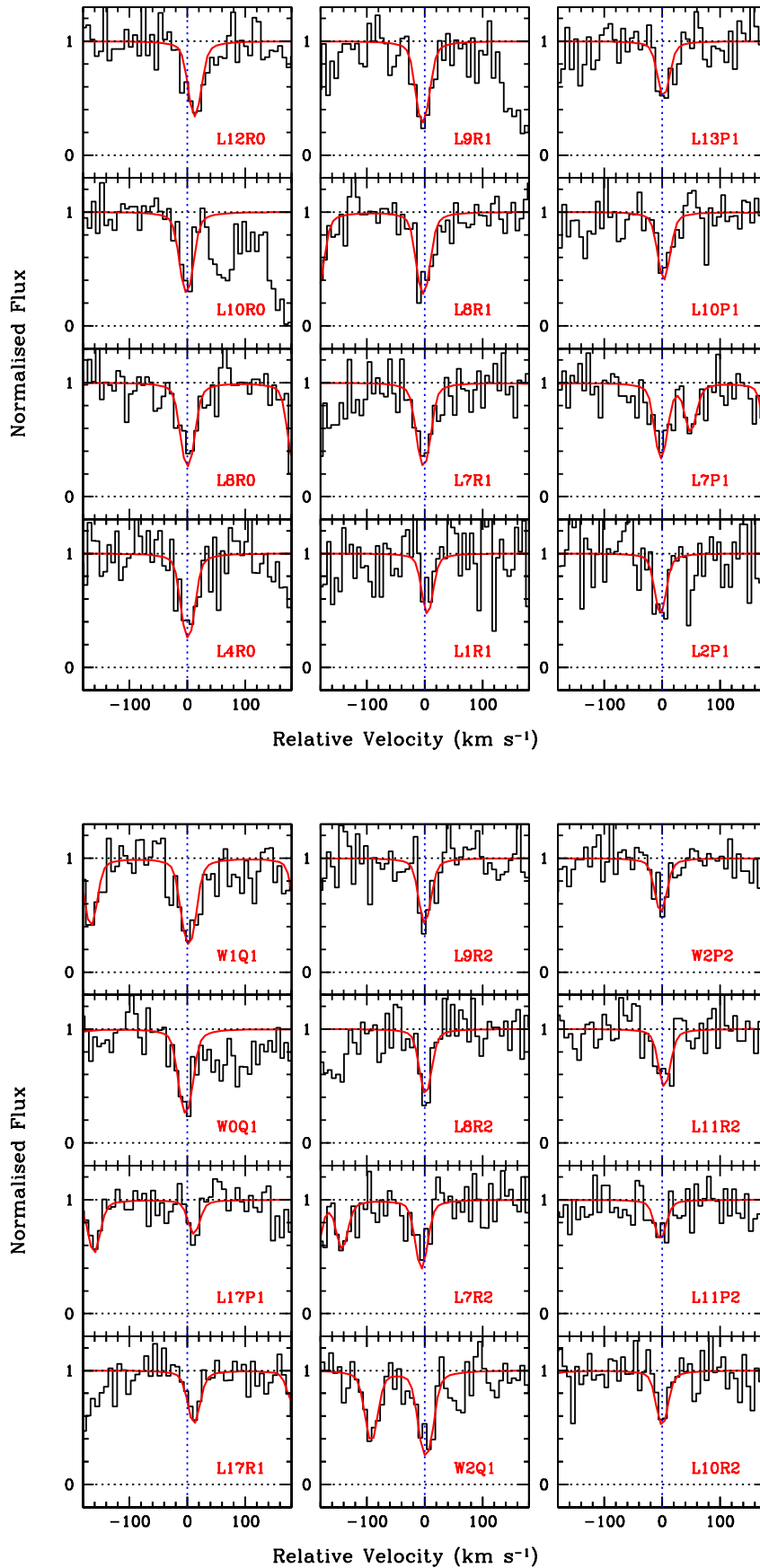


Figure C6. Molecular hydrogen absorption from the  $z_{\text{abs}} = 0.55048$  towards Q1241+176 system.

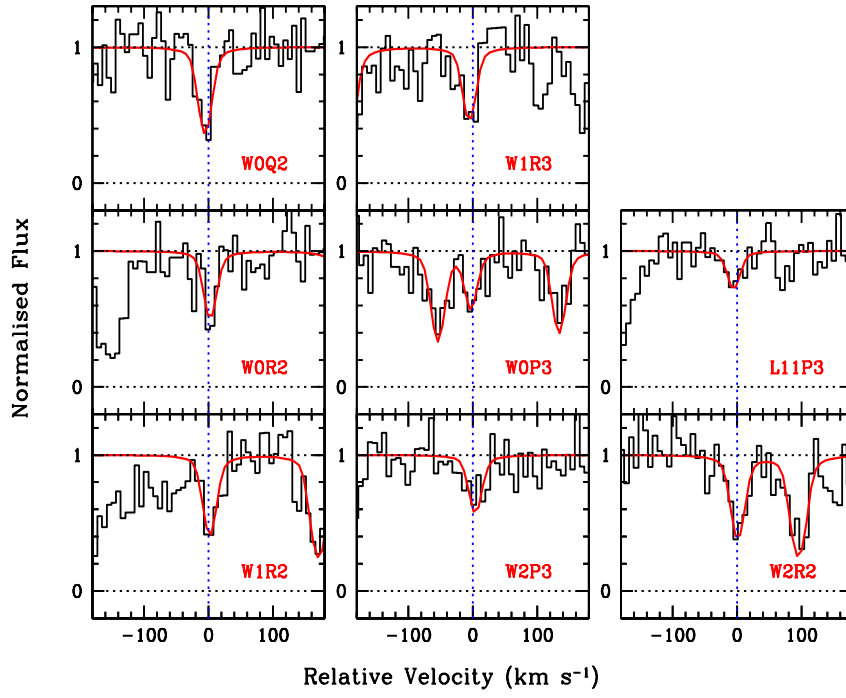


Figure C6. Continued.